Journal of Molecular Structure 1280 (2023) 135086

Contents lists available at ScienceDirect

Journal of Molecular Structure

journal homepage: www.elsevier.com/locate/molstr

Novel thiourea derivative compounds: Thermal behavior, biological evaluation, Hirshfeld surfaces and frontier orbitals analyses, in silico ADMET profiling and molecular docking studies

Tuncay Yeşilkaynak[a,*], Fatma Nur Özkömeç[b], Mustafa Çeşme[c], Ruken Esra Demirdöğen[d], Canan Vejselova Sezer[e], Hatice Mehtap Kutlu[e], Fatih Mehmet Emen[f]

[a] Afsin Vocational School, KahramanmaraşSütcü İmam University, TR46500, Kahramanmaras, Turkey
[b] Department of Biology, Faculty of Arts and Science, KahramanmaraşSütçü İmam University, TR46040, Kahramanmaraş, Turkey
[c] Department of Chemistry, Faculty of Arts and Science, KahramanmaraşSütçü İmam University, TR46040, Kahramanmaraş, Turkey
[d] Department of Chemistry, Faculty of Arts and Science, ÇankırıKaratekin University, TR18100, Çankırı, Turkey
[e] Department of Biology, Faculty of Science, Eskisehir Technical University, TR26555, Eskişehir, Turkey
[f] Department of Chemistry, Faculty of Arts and Science, Burdur Mehmet Akif Ersoy University, TR15030, Burdur, Turkey

ARTICLE INFO

Article history:
Received 31 August 2022
Revised 30 January 2023
Accepted 1 February 2023
Available online 2 February 2023

Keywords:
Thiourea
Thermal behavior
Anticancer activity
Hirshfeld surfaces analysis
Frontier molecular orbital
Molecular docking
ADMET

ABSTRACT

This work reports synthesis and structural characterization of N-(allylcarbamothioyl)-2-chlorobenzamide (HL^1, $C_{11}H_{11}ClN_2OS$) and N-(allylcarbamothioyl)-2-methylbenzamide (HL^2, $C_{12}H_{14}N_2OS$). Structural characterization studies were made via elemental analysis, FT-IR, ^1H NMR and single crystal XRD techniques. Thermal behavior of the synthesized compounds were investigated via TG/DTA. The cell similarity calculation was made. The I_s value for HL^1 and HL^2 was found to be 86.9%. The HL^1 and HL^2 compounds were found to be thermally stable upto 136 and 132 °C, respectively. Anticancer activity of the compounds against MCF-7 breast cancer cells was studied via cell viability test and MTT. The role and the effect of different functional groups present in the compounds on anticancer activity were investigated. The IC_{50} values were found to be in the range 2.59 – 7.09 µmol.L^{-1}. The HL^1 compound showed good antitumor activity at 2.59 µmol.L^{-1} at 48 h. The Hirshfeld surfaces analyses of the compounds were made. The HOMO-LUMO energy levels of HL^1 and HL^2 were calculated. The compounds were thoroughly investigated in silico for their ADMET characteristics. The physicochemical, pharmacological, and ADMET characteristics of HL^1 and HL^2 were investigated together with drug similarity metrics. The compounds were observed to have good drug-like property. Furthermore, molecular docking experiments were carried out to evaluate the interactions between the compoundssynthesized in this study and BRAF (V600E -protein kinase). The acquired results revealed that the synthesized compounds had high binding affinity and inhibitory effect on the BRAF (V600E) protein kinase. The synthesized compounds can be considered potent anticancer agents, according to the data obtained using both in vitro and in silico techniques.

1. Introduction

N,N-dialkyl-*N'*-benzoylthioureas -a group of thiourea derivatives and a very old ligand system- have maintained their preminence with their interesting complexing features. Thioureas have the ability to make hydrogen bonds through the sulfur and nitrogen donor atoms in their structures. These properties affect the behavior of thioureas in various solvents and especially in water [1]. A large number of thiourea derivatives with different properties could be obtained by exploiting the relationship between the hydrogen atoms in thiourea compounds bearing different functional groups. One of the most important features of thethiourea compounds is that they can be easily be synthesized with high yields. Moreover, they have three donor atoms -nitrogen, oxygen and sulfur- with strong electron-donating properties [2]. *N,N*-dialkyl-*N'*-benzoylthiourea ligands can form stable, neutral and often colored chelate compounds with transition metal atoms. The oxidation stability of the *N,N*-Dialkyl-*N'*-benzoylthiourea derivatives is stronger than that of other sulfur binders. The solutions of these compounds obtained in organic solvents are also quite resistant to the oxidizing effect of air. *N,N*-Dialkyl-*N'*-benzoylthiourea derivatives generally can be synthesized via the "Douglass and Dains method", that is, by the "Single Drop Technique" [3]. The thiourea compound is obtained by replacing the sulfur atom in

* Corresponding author.
E-mail address: tyesilkaynak@ksu.edu.tr (T. Yeşilkaynak).

https://doi.org/10.1016/j.molstruc.2023.135086
0022-2860/

the urea molecule with oxygen or by heating the urea in the presence of ammonium rhodanide. Benzoyl thiourea derivative ligands and their metal complexes have wide range of biological activities (i.e., antitumor [4–8], antioxidant [8,9], antiviral [10], antibacterial [8,11–14], antifungal [14,15] and antithyroid [8,13,16]). Studies have shown that thioureas and their compounds can be applied in many different areas due to their interesting properties.

In this study, novel thiourea derivatives-*N*-(allylcarbamothioyl)–2-chlorobenzamide (HL^1, $C_{11}H_{11}ClN_2OS$) and N-(allylcarbamothioyl)–2-methylbenzamide (HL^2, $C_{12}H_{14}N_2OS$) were synthesized. Their crystal structures (HL^1 and HL^2), thermal analysis, antitumor properties and ADMET were studied. The Hirshfeld surfaces analysis of the compounds were studied. The HOMO-LUMO energies of HL^1 and HL^2 were calculated. Moreover, molecular docking analysis was performed to investigate compound-protein interactions. The anticancer potential of the compounds was assessed via in silico approaches.

2. Materials and methods

2.1. Materials and instrumentation

All the chemicals used were of reagent purity and were commercially obtained from Aldrich and Merck. The elemental analyses (C, H, N) was performed using a Costech ECS 410 device. The FT-IR spectra of the compounds were recorded by Perkin Elmer LX-125000B FT-IR instrument and the scanning was made in the range from 400 to 4000 cm^{-1}. The ^1H NMR spectra were obtained via a Bruker Avance III 400 MHz NMR instrument. $CDCl_3$ was used as the solvent and TMS was used as the internal standard. Costech ECS 4010 instrument was used for elemental analyses. Copper and tungsten oxide were used as catalysts to complete the combustion process. The TG/DTA curves were recorded on a SEIKO-II. The single crystals grown from their ethanol solutions were studied via X-ray diffraction analysis. The crystallographic data regarding the ligand was obtained via Bruker D8 Venture single crystal XRD with PHOTON 100 CMOS detector and KryoFlexII low-temperature device operating at 100 K and MoK_α monochromatized radiation (λ=0.71073 Å). Multiscan technique was used to correct the data for absorption effects. Direct methods were used for structural characterization and by using SHELXL 2013 the data was refined on F^2 by full matrix least-squares [17]. The anisotropic displacement parameters were used to refine non-H atoms. Mercury CSD 3.5.1 [18]and Olex2 software [19] was used to prepare the molecular structure plots. The crystal and instrumental parameters were used to determine the unit-cell parameters and also for data acquisition which are given in the supporting information. The crystallographic data of the compounds reported in this paper have been deposited at the Cambridge Crystallographic Data center (CCDC), CCDC 2153424 (HL^1) and CCDC 2153425 (HL^2). Using Bruker SHELXTL Software Package the structure was solved and refined. The compounds with the formula $C_{11}H_{11}ClN_2OS$ (HL^1) and $C_{12}H_{14}N_2OS$ (HL^2) were found to have space group of P-1, crystal system of triclinic and $Z = 2$. Calculations of cell similarity and isostructurality indices by the software ISOS [20,21]. Crystal Explorer 21.5 software was used in Hirshfeld surface analysis [22]. The HOMO-LUMO energies of the HL^1 and HL^2 compounds were calculated using the Gaussian 0.9 software [23] with 6–311++*G* (d,p) basis set [24], B3LYP [25] and ωB97X-D functional [26]. The solvent effect was not taken into account in the DFT calculations. The geometrical optimization of molecules is done in DFT methodology. The pH measurements were made with Mettler Toledo MP 220 pH-meters with a combined electrode with glass electrode as the reference electrode. The accuracy of the pH measurements was found to be ±0.05.

2.2. Synthesis of compounds

2.2.1. Preparation of the compounds

0.01 mol of 2-chlorobenzoyl chloride and 2-methylbenzoyl chloride were dissolved in 50 mL of acetone for to synthesize HL^1 and HL^2, respectively. Then the solutions were added dropwise to 0.01 mol of KSCN in 30 mL acetone and were heated under reflux for 40 min. After cooling to RT, the mixture was mixed with solution of allylamine prepared by dissolving 0.01 mol of allylamine in 10 mL acetone under vigorous stirring for 2 h. Then the reaction mixture was poured onto 300 mL of 0.1 mol.L^{-1} HCl. The precipitate was filtered and was washed with deionized water for several times. The solid product, which was obtained, was recrystallized from $EtOH/CH_2Cl_2$ [27,28]. The reaction scheme for synthesis of HL^1 and HL^2 is shown in Fig. 1.

N-(allylcarbamothioyl)–2-chlorobenzamide (HL^1): Pale brown, *Yield*: 88%, *E. Analysis*: C, 52.3; H, 4.4; N, 10.9; S, 12.3 ($C_{11}H_{11}ClN_2OS$, *calc.* C, 51.9; H, 4.4; N, 11.0; S, 12.6%). FT-IR (ATR, cm^{-1}): υ(N–H) 3243, υ(N–H *ally.*) 3163, υ(C–H *aro.*) 2928, υ(C = O) 1688, υ(C = S) 1152, υ(C–Cl) 743. ^1H NMR ($CDCl_3$): 7.57 (1H, NH), 7.55–7.40 (m, 4H, *Ar*-H), 6.00–5.93 (4H, *Ally*-H), 3.33 (s, 1H, NH) ppm.

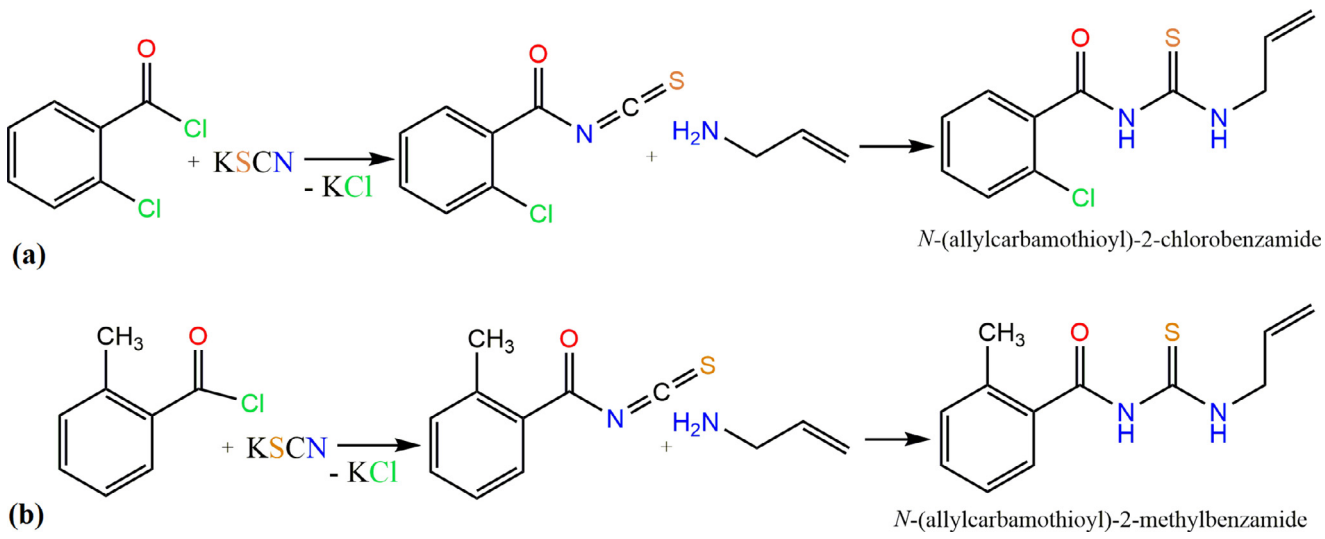

Fig. 1. The reaction scheme for HL^1 (a) and HL^2 (b).

N-(allylcarbamothioyl)−2-methylbenzamide (HL²): Pale yellow, *Yield*: 89%, *E. Analysis*: C, 61.2; H, 5.9; N, 12.2; S, 13.9 ($C_{12}H_{14}N_2OS$, calc. C, 61.5; H, 6.0; N, 12.0; S, 13.7%.) FT-IR (ATR, cm^{-1}): υ(N–H) 3243, υ(N–H *ally.*) 3159, υ(C–H *aro.*) 2985, υ(C = O) 1687, υ(C = S) 1152.^{1}H NMR ($CDCl_3$): 7.57 (1H, NH), 7.56–7.40 (m, 4H, *Ar*-H), 6.00–5.95 (4H, *Ally*-H), 3.33 (s, 1H, NH) ppm.

2.3. Determination of anticancer activity

Anticancer activity studies were performed according to the method reported by Junkyu Han et al. [29]. The standard MTT bioassay was used in vitro cytotoxicity study of the synthesized compounds on cancer cell lines at 24 h and 48 h drug exposure. Human breast cancer cells (MCF-7) were used to determine the promising compounds and for to assess their efficiencies. The MCF-7 cells were purchased from ATCC and were cultured in RPMI-1640 medium containing 10% FBS, 1% 5.000 U/mL of penicillin and 5.000 U/mL Streptomycin under incubation conditions of 5% CO_2 atmosphere at 37 °C. The incubated MCF-7 cells (5×10^3 cells/per well) were seeded on 96 well plates separately for each compound in triplicates and they were further incubated for 24 h and 48 h under the same incubation conditions. Then, the supernatant in each well that contain attached MCF-7 cells were replaced with solutions of test compounds (prepared in RPMI-1640 medium) at different concentrations (3.125, 6.25, 12.50, 25.00, 50 and 100 µmol.L^{-1}) that were placed in separate wells in triplicates according to the labels on the plates. All test plates were incubated for 24 h and 48 h with the compounds at the mentioned concentrations. Then, 20 μL of the MTT solution (5 mg.mL^{-1} in PBS) was added to each well and the plates were incubated for another 4 h. At the end of incubation, the media were carefully removed, and the MTT formazan was dissolved by adding 200 µL of dimethylsulfoxide (DMSO) to each well. The absorbance measurements were performed via a microplate reader for each well at 540 nm. The growth or viability percentages of the treated and untreated cells were calculated by using the formula given below. The half maximal inhibitory concentrations (IC_{50}) were detected from the calculated viability percentages and were used for further experimentations.

$$Growth\ rate = \left(\frac{absorbance\ treated\ wells}{absorbance\ untreated\ wells}\right)x100$$

2.4. In silico ADMET studies

In drug design, determining the pharmaco-kinetic and toxicological properties of the drug candidates is beneficial with respect to time and economic considerations. Absorption, distribution, metabolism, excretion, and toxicity parameters (ADMET) define the properties that a drug molecule should have. The Swiss ADME online database [30]was used to estimate the absorption, distribution, metabolism, and excretion values of the compounds. Web-based platforms pkCSM [31] and ProTox-II online [32] databases were used to estimate the toxicity values. The Smile (smile; formula code of the molecule) notations of synthetic compounds and chemical structures were obtained via ChemDraw 20.0 software. The Smile notations of the compounds were then loged in the SwissADME, pkCSM and ProTox-II to calculate the molecular ADMET properties.

2.5. Molecular docking studies

In molecular docking studies, the optimized structures of the compounds, which were obtained via Gaussian software, were used. The molecular docking studies were performed using PyRx (Autodock Vina) docking software [33,34] to determine the binding energy and interactions of the synthetic compounds with the target protein BRAF (PDB ID: 4R5Y). Throughout this analysis, flexible-ligand: rigid-receptor docking conditions were determined [35,36]. The grid on the ligand-binding pocket of the protein 4R5Y was positioned at the binding site of X:16.93, Y:10.68, Z:−14.56, and the grid size was 29 × 41 × 38 Å^3 dimensions with 0.375 Å. Discovery Studio 2021 was used to analyze and show the findings of the optimum docking positions and the binding affinities for the interactions. A score based on the best-docked protein-ligand complex of the selected compound was obtained from the resulting binding energies (kcal/mol).

3. Results and discussion

3.1. FT-IR

The vibration bands of HL¹ and HL² are given in Table 1. The DFT analysis for FT-IR was performed with 6–311++*G* (d,p) basis set, B3LYP and ωB97X-D functional. The scale factor was not applied to the vibrational frequency values obtained by DFT analysis. The vibration bands obtained from the DFT analysis are also given in Table 1.

The bands observed at 3243 cm^{-1} for HL¹ and 3243 cm^{-1} for HL² in the FT-IR spectra indicate the N–H stretching vibration of the NH_2 group located in the vicinity of the benzene ring. in the DFT analysis for the HL¹ and HL² compounds while the same vibration bands were observed at 3204 cm^{-1} and 3194 cm^{-1} with the B3LYP functional, with the ωB97X-D functional these bands were observed at 3238 cm^{-1} and 3240 cm^{-1}, respectively. The stretching vibration bands of the N–H groups outside the ring in the structure were observed as intense peaks at 3163 cm^{-1} and 3159 cm^{-1} for HL¹ for HL², respectively. In the DFT analysis, while the vibration band was observed at 3149 cm^{-1} for both compounds with B3LYP functional, with ωB97X-D functional these bands were observed at 3144 and 3146 cm^{-1}, respectively. The vibration bands observed at 2928 cm^{-1} and 2985 cm^{-1} indicate the aliphatic C–H stretching vibrations for HL¹ and HL², respectively.

The bands observed in the ranges 1590–1514 cm^{-1} and 1589–1515 cm^{-1} indicate the C–C stretching vibrations in the ring. The intense bands observed at 1426–1031 cm^{-1} for HL¹ and 1425–1031 cm^{-1} for HL² belong to in-plane C–H bending vibrations. The band observed at 743 cm^{-1} (764 cm^{-1} and 753 cm^{-1} with DFT) for HL¹ belong to C–Cl stretching vibrations. The intense bands observed at 1688 cm^{-1} and1687 cm^{-1} for HL¹ and HL², respectively, belong to the stretching vibrations of the carbonyl group (C=O). The bands observed at 1152 cm^{-1} 1152 cm^{-1} for HL¹ and HL², respectively, were attributed to the (C=S) stretching vibration [27,37–43]. In the DFT analysis of both compounds, these vibration bands were observed at 1629 cm^{-1} and 1620 cm^{-1}; 1639 cm^{-1} and 1623 cm^{-1}; 1186 cm^{-1} and 1185 cm^{-1}; 1190 cm^{-1} and 1164 cm^{-1}, respectively. For HL¹ and HL² compounds, the R^2 values obtained from the slope of the graphs drawn between the experimental vibration frequencies and the theoretical frequency values calculated with the B3LYP and ωB97X-D functional were obtained as 0.999, 0.999, 0.998 and 0.999, respectively (**Fig. S1-S4**). These R^2 values obtained from the graph curves show that the B3LYP and ωB97X-D functional used in the DFT calculations are reliable. The FT-IR spectra of HL¹ and HL² are given in the supplementary data (**Fig. S5** and **Fig. S6**). The FT-IR spectra and the spectral data of HL¹ and HL² obtained by the DFT analysis are given in the supplementary data (**Table S1,Table S2,Fig. S7-S10**).

3.2. ^{1}H NMR

The ^{1}H NMR spectra of the HL¹ and HL² compounds confirm their proposed structures. The two peaks observed at 7.57 ppm

Table 1
The experimental and theorical FT-IR vibrational frequency (unscaled) of HL^1 and HL^2.

Compound	*NearAro-* ν(N–H)	*NearAli-*ν(N–H)	ν(C–C)	ν(C–H)	ν(C = O)	ν(C = S)	ν(C–Cl)
HL^1 (Exp.)	3243	3163	1590,1514	1426,1031	1688	1152	743
HL^2 (Exp.)	3243	3159	1589,1515	1425,1031	1687	1152	–
HL^1 (B3LYP)	3204,3605	3149,3451	1588,1500	1453,1030	1629	1186	764
HL^2 (B3LYP)	3194,3611	3149,3445	1544,1494	1453,1032	1639	1190	–
HL^1 (ωB97X-D)	3238,3649	3144,3522	1566,1522	1414,1055	1620	1185	753
HL^2 (ωB97X-D)	3240,3655	3146,3509	1571,1503	1413,1057	1623	1164	–

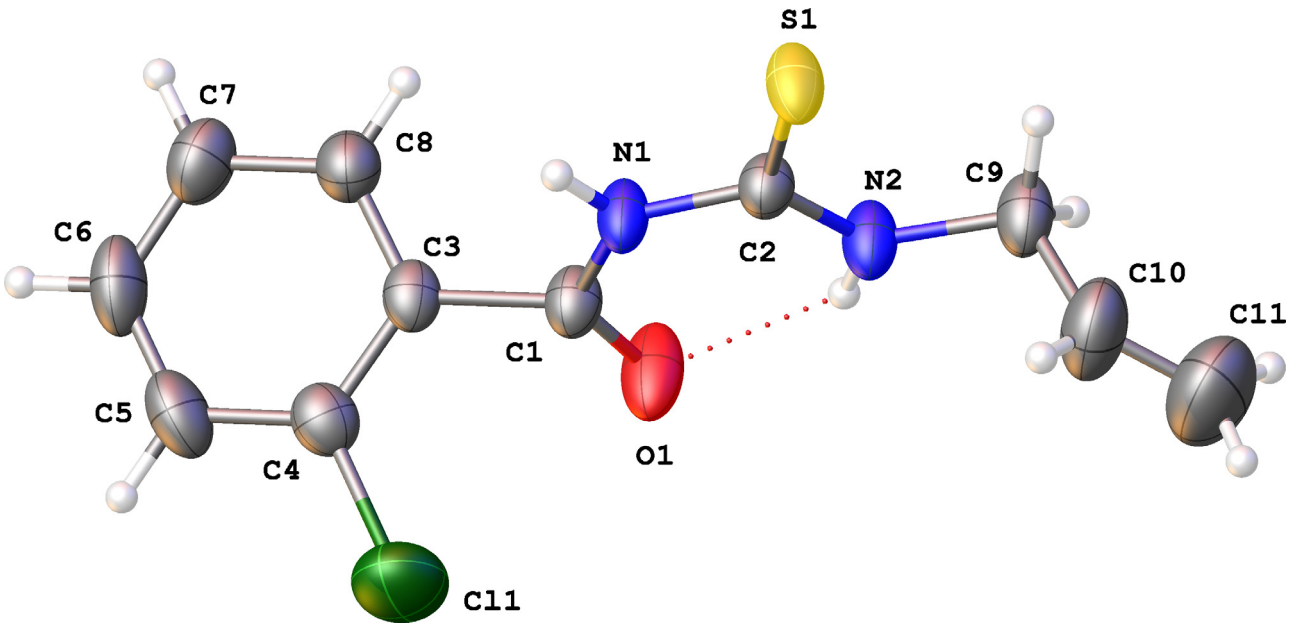

Fig. 2. ORTEP view of the HL^1; thermal ellipsoids are shown at the 50% probability level.

(ali.) and 3.33 ppm (ali.) for HL^1 indicate the N–H group. While the multiplet peaks observed at around 7.55–7.40 ppm with HL^1 indicate the C–H bonds in the aromatic ring, the multiplet peaks observed at around 6.00–5.93 ppm indicate the C–H bonds in the aliphatic chain. The two peaks observed in the ^{1}H NMR spectrum of the HL^2 at 7.57 ppm (ali.) and 3.33 ppm (ali.) indicate the N–H group. The C–H bonds in the aromatic ring were observed to appear as multiplet peaks at around 7.56–7.40 ppm for HL^2. The C–H bonds in the aliphatic chain were observed to appear as multiplet peaks at around 6.00–5.95 ppm for HL^2 [41]. The ^{1}H NMR spectra of HL^1 and HL^2 are given in the supplementary data (**Fig. S11** and **Fig. S12**). The DFT analysis for ^{1}H NMR was performed with 6–311++*G* (d,p) basis set, B3LYP, CSGT functional. In the DFT analysis, while the N–H peaks were observed at 3.74 and 3.78 ppm for the HL^1 compound for the HL^2 compound these peaks were observed at 3.99 and 3.88 ppm. The peaks observed at 4.84–5.18 ppm and at 5.12–5.28 ppm for HL^1 and HL^2, respectively, were attributed to the C–H bond in the benzene rings in the structures of these compounds. The data obtained by DFT analysis for the ^{1}H NMR spectra of HL^1 and HL^2 are given in the supplementary data (**Table S3).**

3.3. Crystallographic structure of the ligands

The molecular structures of HL^1 and HL^2 with the atom numbering schemes (ORTEP view) are given in Fig. 2 and Fig. 4. The crystal data and the structure refinement parameters of HL^1 and HL^2 are given in Table 2 and Table 3. Some experimental geometric parameters are given in the supporting information. In the X-ray crystallographic analysis, approximate dimensions of 0.100 mm x 0.100 mm x 0.050 mm and 0.100 mm x 0.100 mm x 0.100 mm were used for HL^1 and HL^2, respectively. The frames were integrated with the Bruker SAINT software package using a wide-frame algorithm. The structures were solved and refined via the Bruker SHELXTL Software Package by using the space groups P-1.

Table 2
Crystal data and structure refinement parameters of HL^1.

Empirical formula	$C_{11}H_{11}ClN_2OS$
Formula weight	254.73
Temperature/°K	297.11
Crystal system	Triclinic
Space group	P-1
a/Å	6.8364(5)
b/Å	8.6935(7)
c/Å	10.6293(7)
α/°	91.598(4)
β/°	98.663(4)
γ/°	91.948(4)
Volume/Å^3	623.81(8)
Z	2
ρ_{calc}g/cm^3	1.356
μ/mm^{-1}	0.454
F(000)	264.0
Crystal size/mm^3	0.1 × 0.1 × 0.05
Radiation	MoKα (λ = 0.71073)
2Θ range for data collection/°	5.986 to 56.568
Index ranges	$-9 \le h \le 9$, $-11 \le k \le 11$, $-14 \le l \le 14$
Reflections collected	20,849
Independent reflections	3090 [R_{int} = 0.0698, R_{sigma} = 0.0533]
Data/restraints/parameters	3090/0/145
Goodness-of-fit on F^2	1.029
Final R indexes [I>=2σ (I)]	R_1 = 0.0523, wR_2 = 0.1122
Final R indexes [all data]	R_1 = 0.1074, wR_2 = 0.1367
Largest diff. peak/hole / e Å^{-3}	0.30/−0.33

Table 3
Crystal data and structural refinement parameters of HL^2.

Empirical formula	$C_{12}H_{14}N_2OS$
Formula weight	234.31
Temperature/K	273.15
Crystal system	Triclinic
Space group	P-1
a/Å	6.8736(2)
b/Å	8.6153(3)
c/Å	10.6652(4)
α/°	91.541(2)
β/°	98.127(2)
γ/°	91.147(2)
Volume/Å^3	624.82(4)
Z	2
ρ_{calc}g/cm^3	1.245
μ/mm^{-1}	0.240
F(000)	248.0
Crystal size/mm^3	0.1 × 0.1 × 0.1
Radiation	MoKα (λ = 0.71073)
2Θ range for data collection/°	5.988 to 57.28
Index ranges	$-9 \le h \le 9$, $-11 \le k \le 11$, $-14 \le l \le 14$
Reflections collected	22,599
Independent reflections	3203 [R_{int} = 0.0433, R_{sigma} = 0.0297]
Data/restraints/parameters	3203/0/155
Goodness-of-fit on F^2	1.023
Final R indexes [$I>=2\sigma$ (I)]	R_1 = 0.0409, wR_2 = 0.0972
Final R indexes [all data]	R_1 = 0.0638, wR_2 = 0.1089
Largest diff. peak/hole / e Å^{-3}	0.21/−0.19

The crystal packing is given in Fig. 3. An intramolecular hydrogen interaction can be observed here (N–H… O) [43,44]. The bond length of H…O was found to be 2.018 Å. For HL^1, the lengths of the N…O and N–H bond were 2.690 Å and 0.860 Å, respectively, and the N–H…O angle was 134.40°.

According to the results obtained in the structural analysis, the bond lengths of S1-C2 and O1-C1 were found to be 1.672(3) and 1.208(3) Å, respectively. These results that lie in the typical average double bond length suggest existence of a double bond. The bond lengths of the N1-C2, 1.396(3); N2-C2, 1.321(3) and N1-C1, 1.368(3) Å are indicative of a partial double bond. The bond angles of the C = O and C=S groups were determined. For N1-C2-S1 the bond angle was 118.19(16)º. For N2-C2-S1 it was 125.02(17)º. For N1-C1-O1 its was 123.50(2)º and for O1-C1-C3 it was 122.30(2)º.

The proposed crystal structure of the HL^2 is presented in Fig. 4. The crystal parameters are presented in Table 3. An intramolecular hydrogen interaction was observed here (N–H…O). The bond length of H…O is 2.028 Å [43,44]. In the HL^2 molecule, lengths of the N…O and N–H bonds were 2.698 Å and 0.860 Å, respectively, and the N–H…O angle was 134.12°. The necessary parameters are given the supporting file (**Table S4-S17**).

The crystal packing is shown in Fig. 5. The results obtained in the structural analysis indciated that the bond lengths for C2-S1 and C1-O1 were 1.6753(15) and 1.2197(18) Å, respectively. These results, which lie in the typical average double bond length, suggest a double bond. The bond lengths of N1-C1, N1-C2, and N2-C2, which were 1.3690(19); 1.3967(18) 1.3207(19) Å, respectively, were indicative of partial double bond. The bond angles of C=O and C=S groups are N2-C2-S1, 124.94°(11); N1-C2-S1,118.04° (10); N1-C1-O1, 122.93° (14) and O1-C1-C3, 122.51°(13) .

The cell similarity calculation was made with the ISOS software. The similarity between the unit cells of two crystal structures is a prerequisite to indicate their similarity. The cell similarity index (π) describes the dissimilarity of the unit cell dimensions of the crystal structures that are compared:

$$\pi = \left| \frac{a+b+c}{a'+b'+c'} - 1 \right|$$

Here, the orthogonalized lattice parameters of the two related crystals are indicated with the letters a, b, and c and a′, b′, and c′, respectively. As the similarity of the two unit cells increases the value of π would be closer to zero [20,21]. Using the above given equation the π values for HL^1 and HL^2 crystals were calculated to be approximately 0.011. This value is indicative of the reveals that the probability of the isostructurality of two crystal structures be is very high. The isostructurality index (Is) of two related crystal structures can be calculated as follows:

$$I_s(n) = \left| \left[\frac{\Sigma(\Delta Ri)^2}{n} \right]^{1/2} - 1 \right| x100\%$$

where n is the number of related non-hydrogen atoms, and ΔR_i are the distance differences between their atomic coordinates. The isostructurality index takes into account both the differences of the molecular geometries and the molecular positional differences caused by rotations or translations. In the event of high structural similarity, I_s is becoming close to 100% [20,21]. The I_s value for HL^1 and HL^2 was found to be 86.9%.

3.4. Thermal characterization of the compounds

The DTA-TG analysis of the compounds of sample mass in the range 9.00–10.00 mg were performed at a heating rate of 10 °C/min under N_2 atmosphere. The results obtained in the DTA-TG study of $HL^1$are given in Fig. 6. The thermal degradation of HL^1 occurs in two steps and the compound disintegrates into some small fragments. The first degradation step took place with an experimental mass loss of 20.00% (22.06% calculated) in the temperature range from 136 °C to 226 °C (Tp:149 °C). In the first step, the aliphatic group of the compound -the $C_3H_6N\cdot$ radical- is detached from the structure and an intermediate structure, which was proposed to be $C_8H_5ClNOS,\cdot$was formed. The second degradation step was observed above 226 °C (T_p:244 °C) with a mass loss of 80.00%. In this step, the intermediate product decomposes into smaller fragments (CO, CS, NO etc.) in gas phase. After the second degradation step, the ligand was observed to completely decompose [38,43,45].

The result of the DTA-TG study of HL^2 is given in Fig. 7. HL^2 degraded in two steps. The first degradation step was observed in the range from 132 °C to 199 °C (T_p:148 °C). In this step, 0.15 mol of the compound was found to leave the structure. This corresponds to an experimental mass loss of 15.00% (calc.%17.53). In the first step of thermal degradation, the aliphatic group of the ligand -the $C_3H_5\cdot$ radical- was found to leave the structure.The chemical formula of the intermediate product formed at the end of the first step was proposed to be $L_{0.85}$ ($C_9H_9N_2OS\cdot$). The second degradation step took place above199 °C (T_p:238 °C) with an experimental mass loss of 85.00%. In this step, 0.85 mol of the ligand was found to leave the structure and turn into gaseous products. After the second degradation step, the ligand completely degraded [38,43,46].

3.5. Anticancer activities

The MTT assay was used to investigate the cytotoxic effect of the compounds against the MCF-7 human breast cancer cells via the method proposed by Han et al. [29]. Cell viability was determined via spectrophotometric method and the IC_{50} value of each compound on the MCF-7 cells was determined. The viability percentages of the MCF-7 cells upon treatment with the compounds for 24 h and 48 h are presented in Tables 4 and 5. The highest decrease in growth or to state in another way in inhibition was observed when the compounds were applied at the highest concentration which was 100 µmol.L^{-1}. Growth inhibition over 24 h was

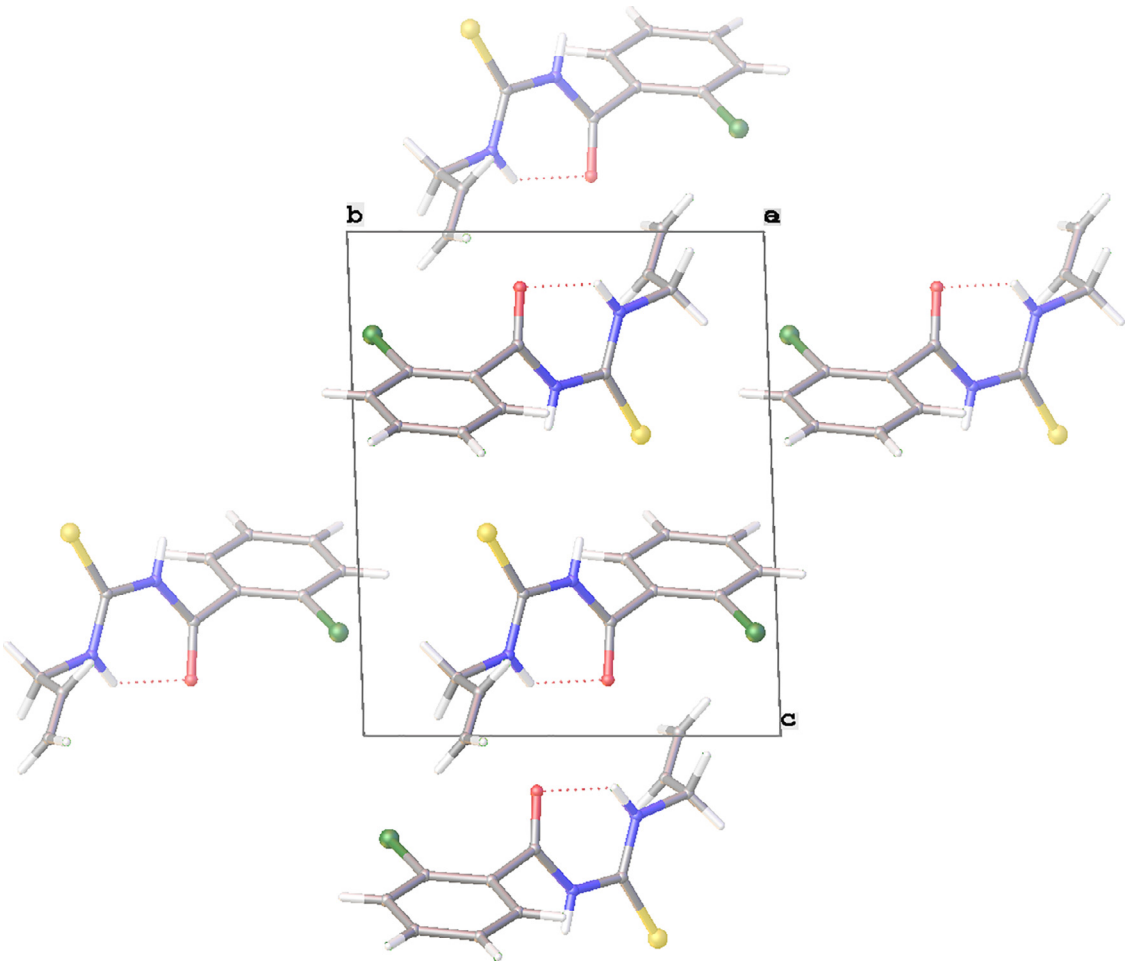

Fig. 3. Crystal packing of the HL^1 in triclinic system with P-1 space group.

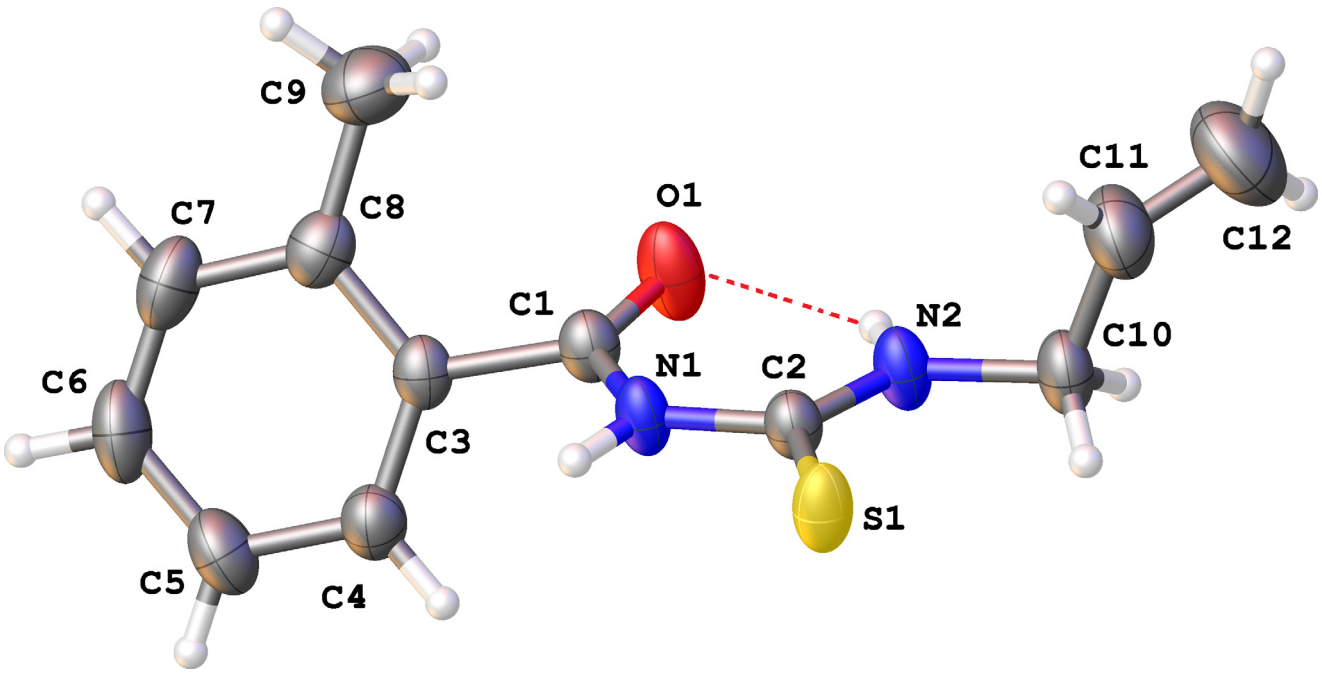

Fig. 4. ORTEP view of the HL^2; thermal ellipsoids are shown at the 50% probability level.

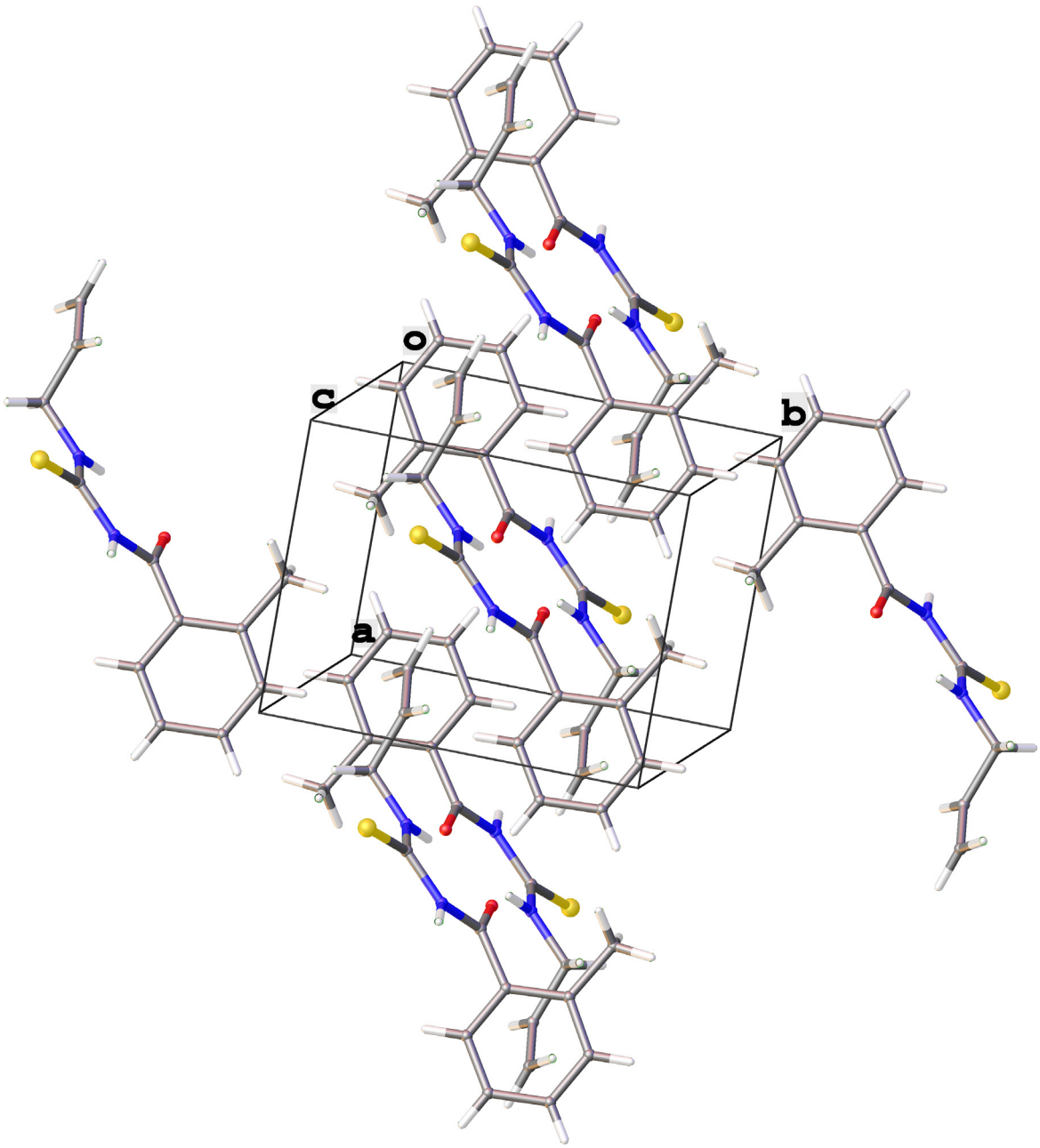

Fig. 5. Crystal packing of the HL^2 in triclinic system with P-1 space group.

Table 4
The viability percentages of MCF-7 cells after treatment with HL^1 and HL^2 for 24 h.

24h	HL^1		HL^2	
Doses (µmol.L^{-1})	Viability (%)	Standard Deviation(±)	Viability (%)	Standard Deviation(±)
100	19.93	1.48	2.50	4.04
50	23.60	7.17	13.57	2.02
25	26.75	7.66	15.89	1.77
12.5	25.52	6.92	17.86	1.52
6.25	28.50	2.23	23.75	1.26
3.125	23.43	0.99	101.25	1.77
Control	99.65	0.99	96.43	2.53
IC_{50} (µmol.L^{-1})	4.36		3.99	

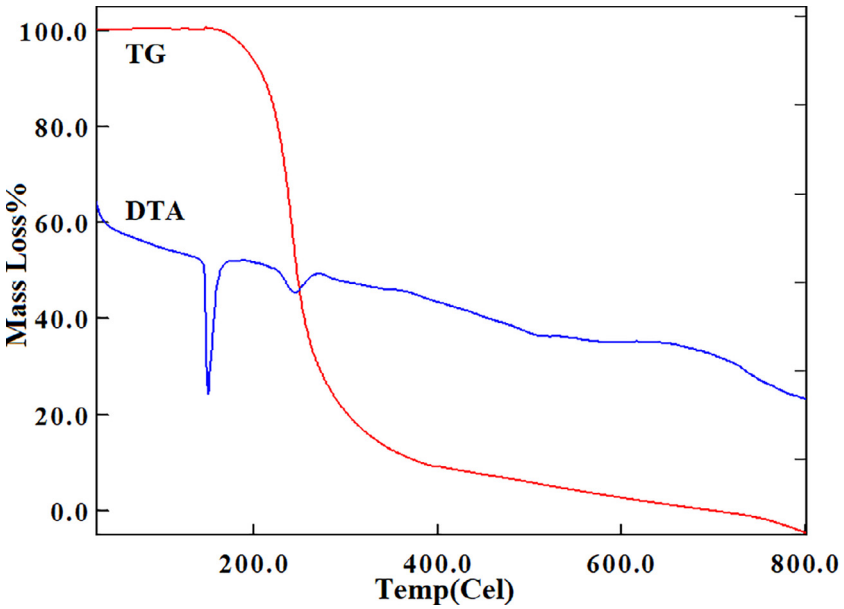

Fig. 6. The DTA-TG diagrams of HL^1.

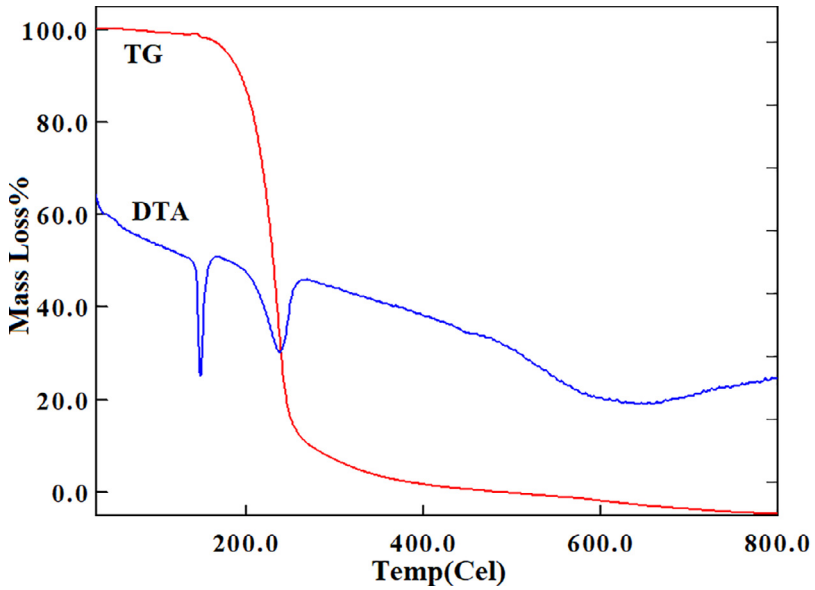

Fig. 7. The DTA-TG diagrams of HL^2.

observed to be stronger when HL^2 and HL^1 compounds were at low concentrations namely 6 and 25 µmol.L^{-1}, respectively. However, over 24 h of application, when the concentrations of the compounds HL^2 and HL^1 were the lowest namely 3 and 125 µmol.L^{-1}, respectively, the maximum inhibition was observed to be lowest. Over 24 h of application, the IC_{50} values for the compounds HL^1 and HL^2 were determined to be 4.36 and 3.99 µmol.L^{-1}, respectively (Table 4, Fig. 8). In a similar way, when the MCF-7 cells were treated with HL^1 and HL^2 compounds for 48 h, a sharp decrease was observed in the viability of the cells. After treating the MCF-7 cells with the compounds for 48 h, the IC_{50} values of HL^1 and HL^2 were found to be 2.59 and 7.09 µmol.L^{-1}, respectively (Table 5, Fig. 8). The results obtained in the MTT test indicate that the cytotoxicity/anticancer activity of HL^1 and HL^2 compounds are time- and dose-dependent.

HL^1 showed better anticancer activity at 48 h with an IC_{50} value of 2.59 µmol.L^{-1}. The IC_{50} value of HL^2, which is 3.99 µmol.L^{-1}, indicated that this compound has good anticancer activity at 24 h. After 24 h of application, the IC_{50} value for HL^1, which was 4.36 µmol.L^{-1}, indicated that HL^1 also had considerable antitumor activity. Thus, the antitumor activity of HL^1, when applied for 24 h and 48 h, and the activity of HL^2, when applied for 24 h,was found to be stronger than that of 5-fluorouracil (5-FU) – a widely used agent in cancer treatment- the IC_{50} value of which was 4.7 µmol.L^{-1} [47].

3.6. Hirshfeld surfaces analysis

Hirshfeld surfaces of the compounds mapped with d_i, d_e and d_{norm} shape index functions are given in Fig. 9 and Fig. 10, which also shows the surfaces mapped on the dnorm with a fixed color scale of (−0.338) - (+1.444) Å for HL^1 and (−0.312) - (+1.430) for HL^2. The dnorm surface is used to describe interactions between the molecules in close proximity, and the surface is mapped in a

Table 5
The viability percentages of MCF-7 cells after treatment with HL^1 and HL^2 for 48 h.

48h	HL^1		HL^2	
Doses (µmol.L^{-1})	Viability (%)	Standard Deviation(±)	Viability (%)	Standard Deviation(±)
100	14.46	4.80	8.29	3.52
50	23.93	3.03	25.55	0.20
25	31.07	2.02	36.19	2.34
12.5	34.11	3.28	41.99	1.56
6.25	40.36	7.58	51.24	1.76
3.125	39.64	1.52	57.04	0.20
Control	99.82	0.00	100.14	10.35
IC_{50} (µmol.L^{-1})	2.59		7.09	

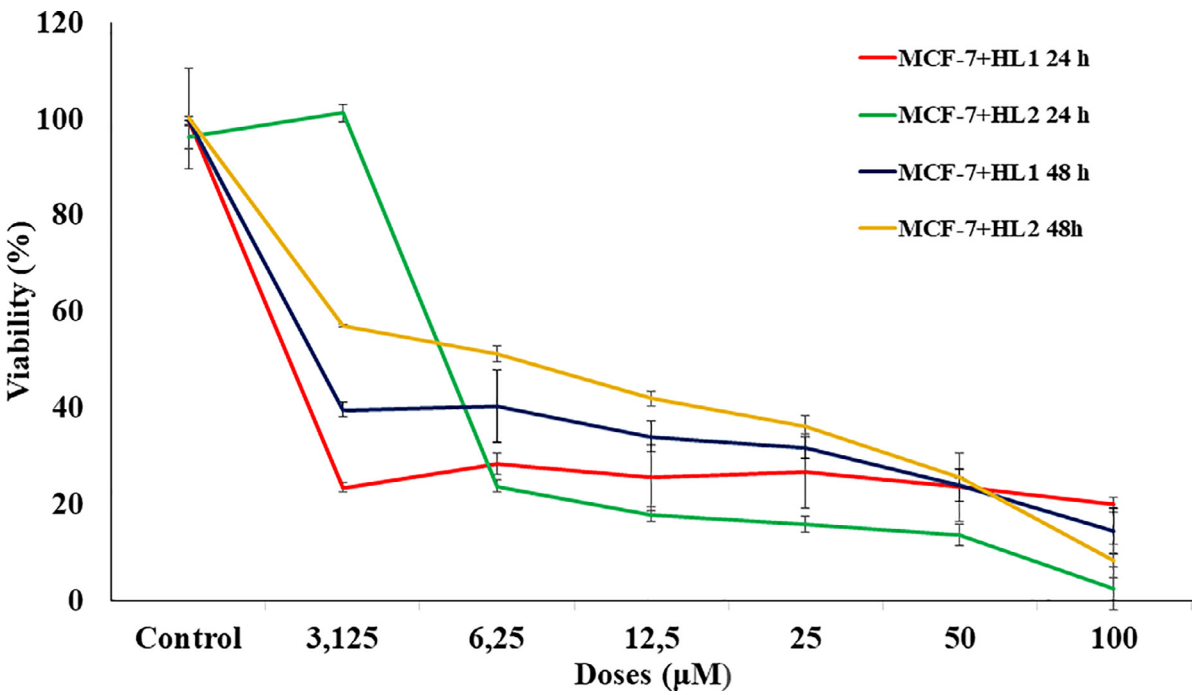

Fig. 8. The growth inhibition caused by HL^1 and HL^2 on MCF-7 cells for 24 and 48 h of application.

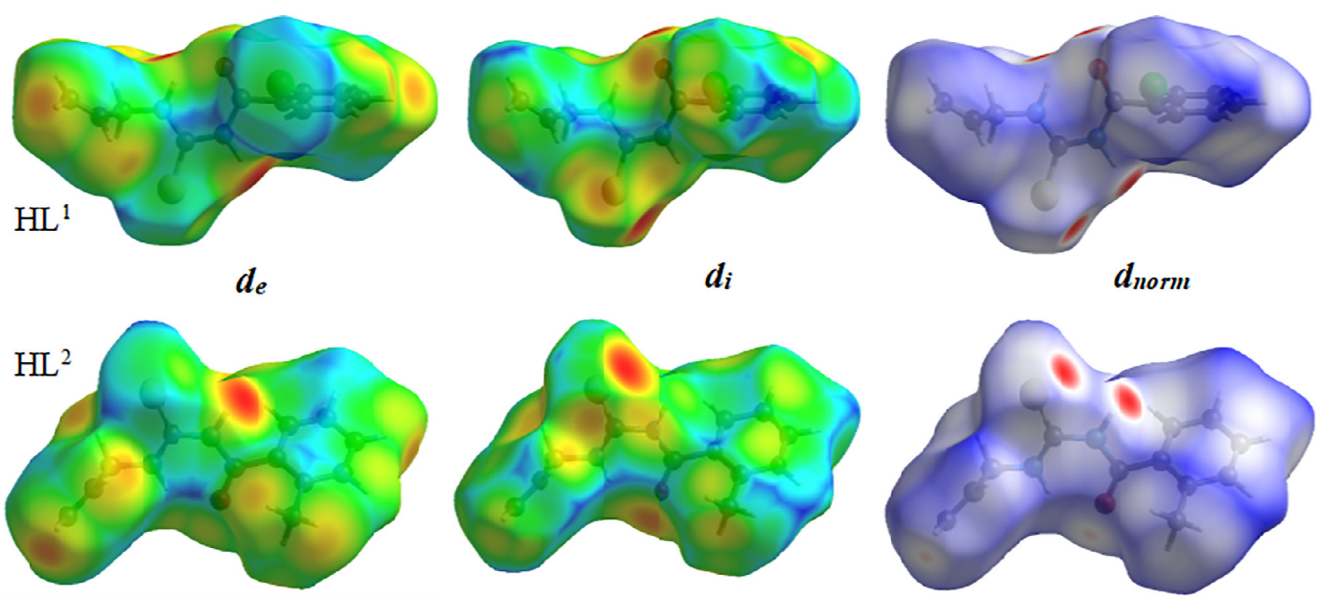

Fig. 9. The Hirshfeld surfaces of HL^1 and HL^2 compounds mapped with de, di and dnorm shape index functions.

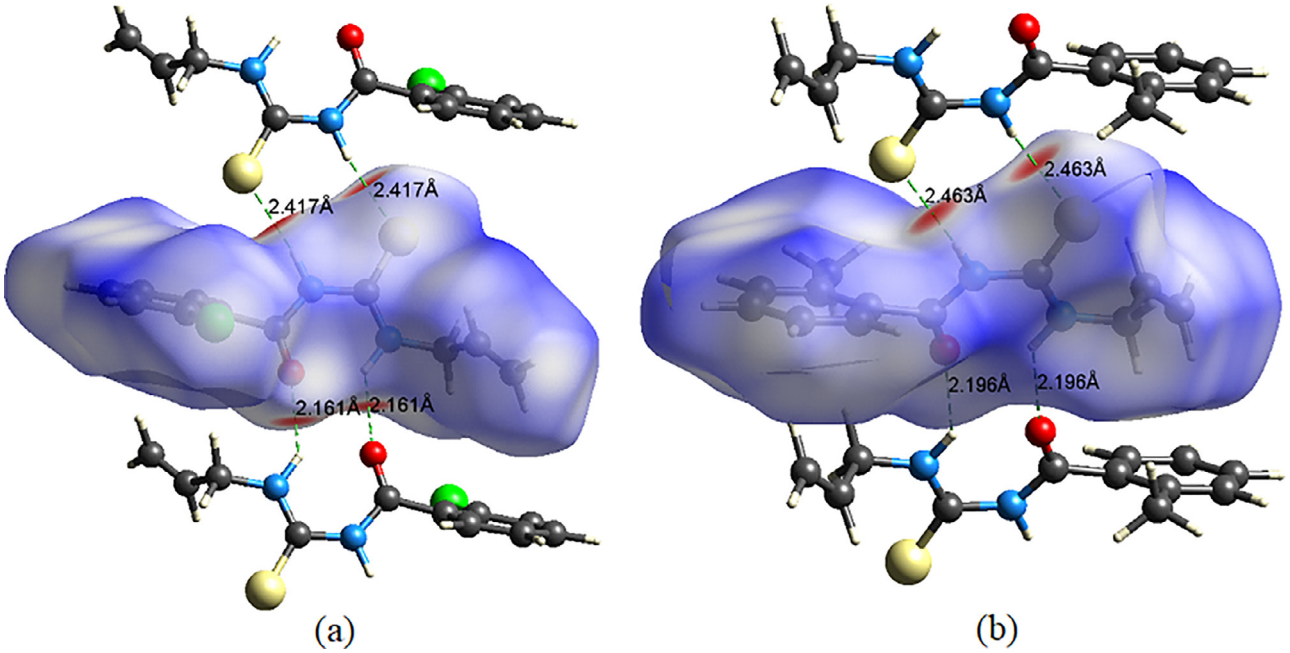

Fig. 10. The H…S and H…O interaction distances for HL^1 (a) and HL^2 (b).

red-blue-white color scheme. The red areas indicate closer contacts than the van der Waals (vdW) radia, the blue areas indicate the interactions farther than the van der Waals radia and the white areas indicate the interactions within the van der Waals radia distance. The shape indexes are often used to determine the characteristic packing and stacking modes and the way the neighboring molecules come into contact with each other.

The Hirshfeld surfaces mapped with dnorm functions for HL^1 and HL^2 are given in Fig. 10. The visible bright red regions on the dnorm surface represent N–H…S and N–H…O interactions. The interaction distances of H…S and H…O in HL^1 were 2.417 Å and 2.161 Å, respectively. In HL^2, these distances were 2.463 Å and 2.196 Å, respectively.

The 2D and disaggregated fingerprint graphs of the compounds show all the intermolecular interactions of the Hirshfeld surface. The fingerprint plots for compound HL^1 are given in Fig. 11.

The 2D fingerprint plots of the HL^1 revealed the presence of H..H, C..H/H..C, H..Cl/Cl..H, H..S/S..H and H..O/O..H interactions in the compound. The H..H interaction with 34.4% probability among all the interactions was the strongest interaction. The intensity was in the middle regions of the fingerprint plot. The contribution of the C..H/H..C interactions to the total Hirshfeld surfaces was 17.9%. There are also H..Cl/Cl..H, H..S/S..H and H..O/O..H interactions in the compound and the contribution of these interactions were found to be 15.9%, 13.9% and 10.20%, respectively. The fingerprint plots for HL^2 are given in Fig. 12.

The 2D fingerprint plots for HL^2 revealed the presence of H..H, C..H/H..C, H..S/S..H and H..O/O..H interactions in the compound. Among all the interactions, the probability of the H..H interaction, which was 53.4%,.was very high. The density was in the middle regions of the fingerprint graph. The contribution of the C..H/H..C interactions to the total Hirshfeld surfaces was 18.2%. The H..S/S..H and H..O/O..H interactions were also found to be present in the compound and the contribution of these interactions were 14.1% and 8.90%, respectively. The predominant N–H..S H bonding interactions in HL^1 and HL^2 appeared as two spikes in the 2D fingerprint plot showing the S..H/H..S interactions (Fig. 11 and Fig. 12). In the 2D fingerprint graph of the S..H/H..S interactions, the molecule acts as a donor at the $d_i > d_e$ peak, and the molecule acts as an acceptor at the $d_e > d_i$ peak. The all non-covalent interactions of HL^1 and HL^2 molecules with van der Waals radii of 3.50 Å are given in Fig. 13 and Fig. 14.

3.7. Frontier molecular orbitals analysis

The HOMO and LUMO energy values are very important parameters in terms of quantum chemistry of compounds. While the LUMO accepts electrons,;the HOMO, which is the outermost orbital and tends to give electrons, acts as an electron donor. The HOMO-LUMO energies of HL^1 and HL^2 were calculated by using the Gaussian 0.9. The DFT analysis and this was performed with 6–311++*G* (d,p) basis set, B3LYP and ωB97X-D functional. The ωB97X-D functional is a range separated functional that can describe charge transfer system more accurately than B3LYP. The ωB97X-D functional uses a dispersion model [26]. The B3LYP is the hybrid functional used especially for the short range interactions.

Using the B3LYP functional, the HOMO and LUMO energy levels of HL^1 were calculated to be −0.22653 eV and −0.06641 eV, respectively. Using the ωB97X-D functional, the HOMO and LUMO energy levels of HL^1 were calculated to be −0.30416 eV and −0.00172 eV, respectively. Using the B3LYP functional, the HOMO and LUMO energy levels of HL^2 were calculated to be −0.22477 and −0.06199 eV, respectively. Using the B3LYP functional, the HOMO and LUMO energy levels of HL^1 were calculated to be −0.30108 and −0.00273 eV, respectively. The HOMO-LUMO transition energy difference for HL^1 and HL^2 were found to be 0.16012 eV and 0.16278 eV with B3LYP functional (Fig. 15). Also, the HOMO-LUMO transition energy difference for HL^1 and HL^2 were found to be −0.30244 and −0.29835 eV with ωB97X-D functional, respectively.

Depending on the substituents, different band gap values are reported for benzoylthioureas in the literature. For instance, while the HOMO-LUMO band gaps for N-((4-acetylphenyl)carbamothioyl)pivalamide, N,N-di-2,4-dimethoxybenzyl-N'−2-nitrobenzoyl thiourea and 1-(adamantane-1-carbonyl-3-(1-naphthyl)) thiourea ($C_{22}H_{24}N_2OS$) were calculated to be 0.1284 eV [48], 0.8033 eV [49] and 1.65 eV [50], respectively.

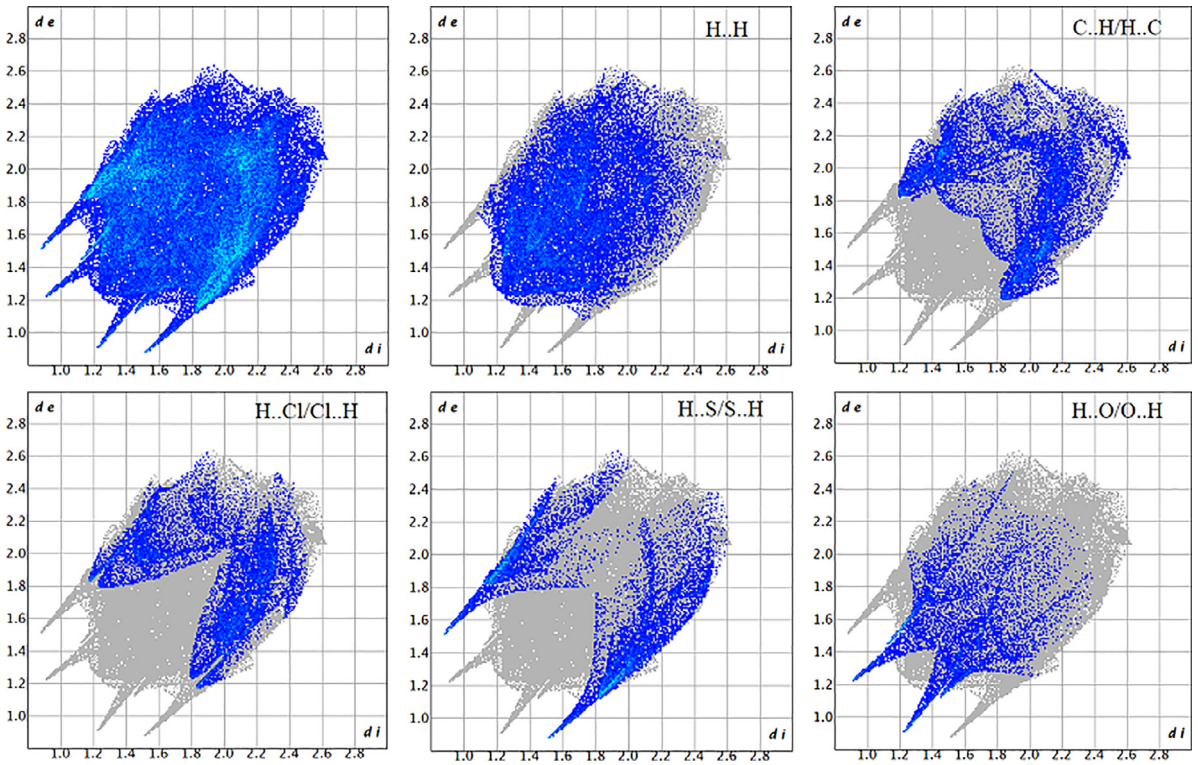

Fig. 11. The fingerprint plots for HL^1.

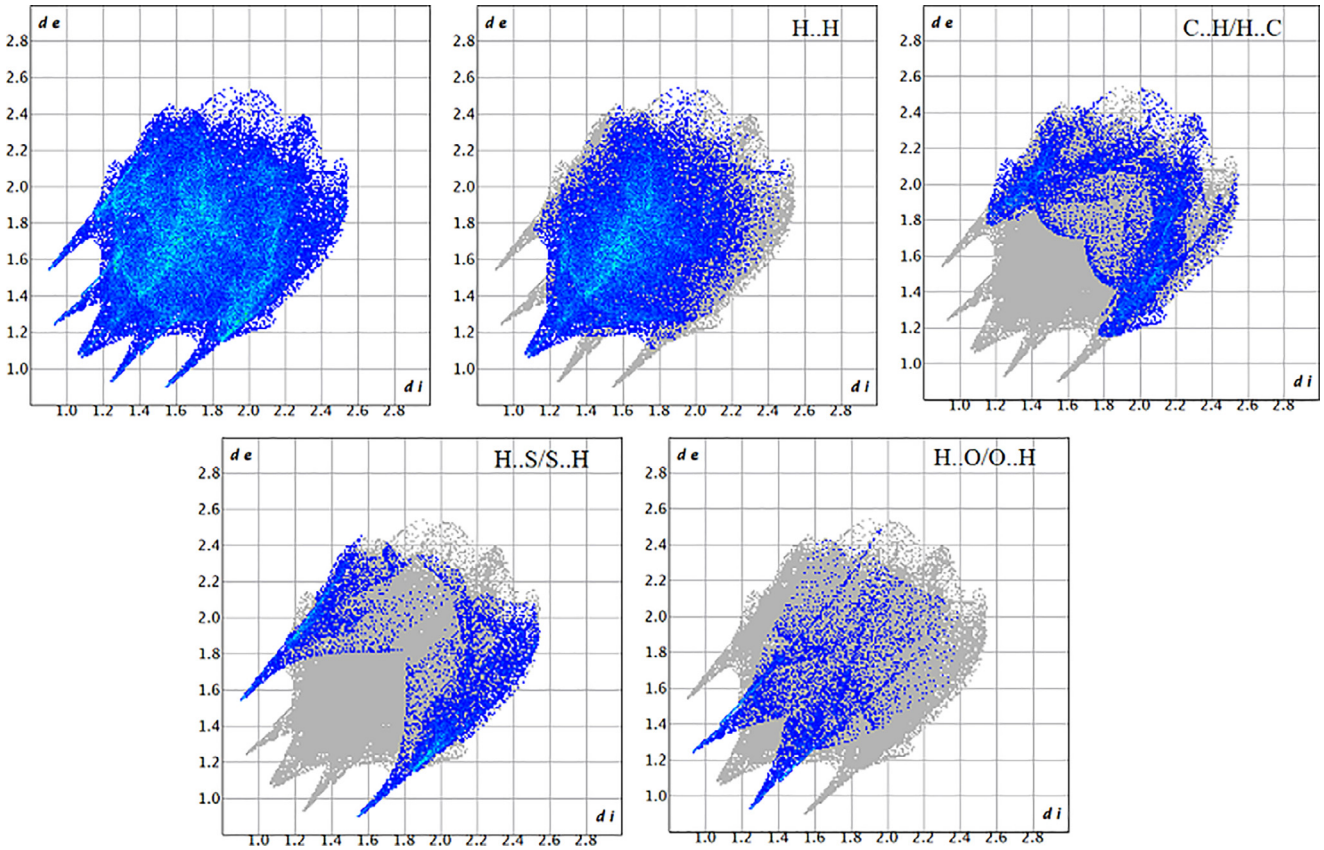

Fig. 12. The fingerprint plots for HL^2.

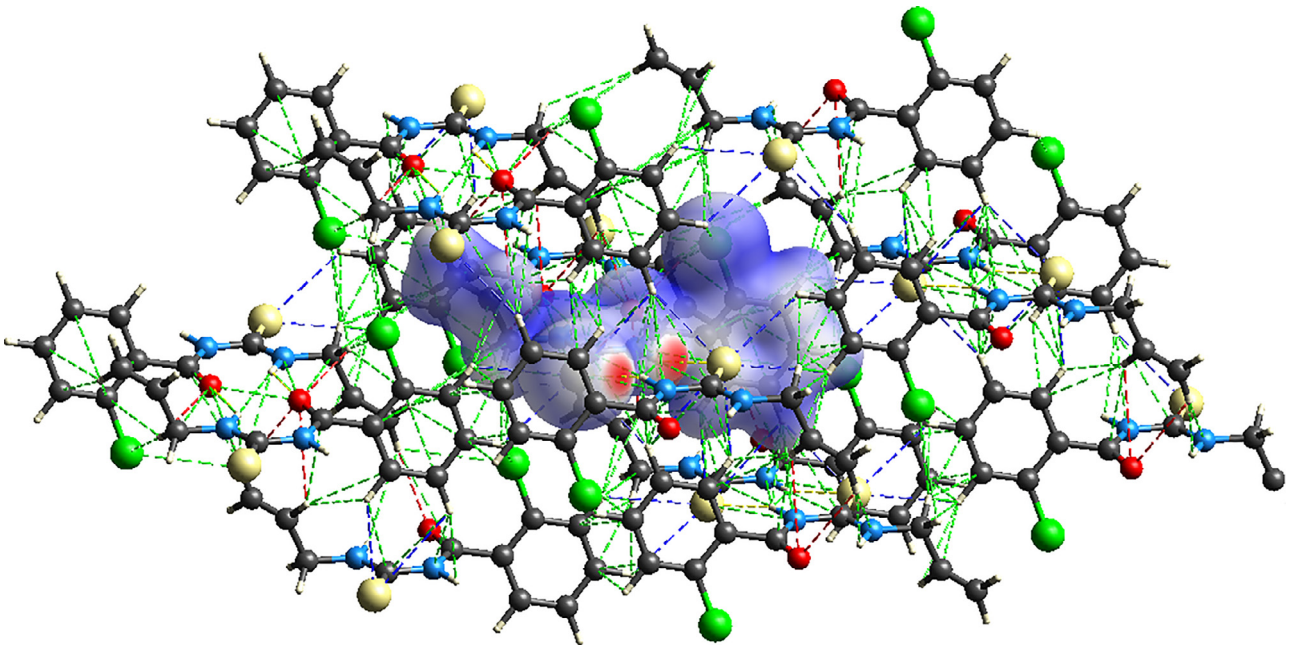

Fig. 13. The non-covalent interactions of HL^1 molecules.

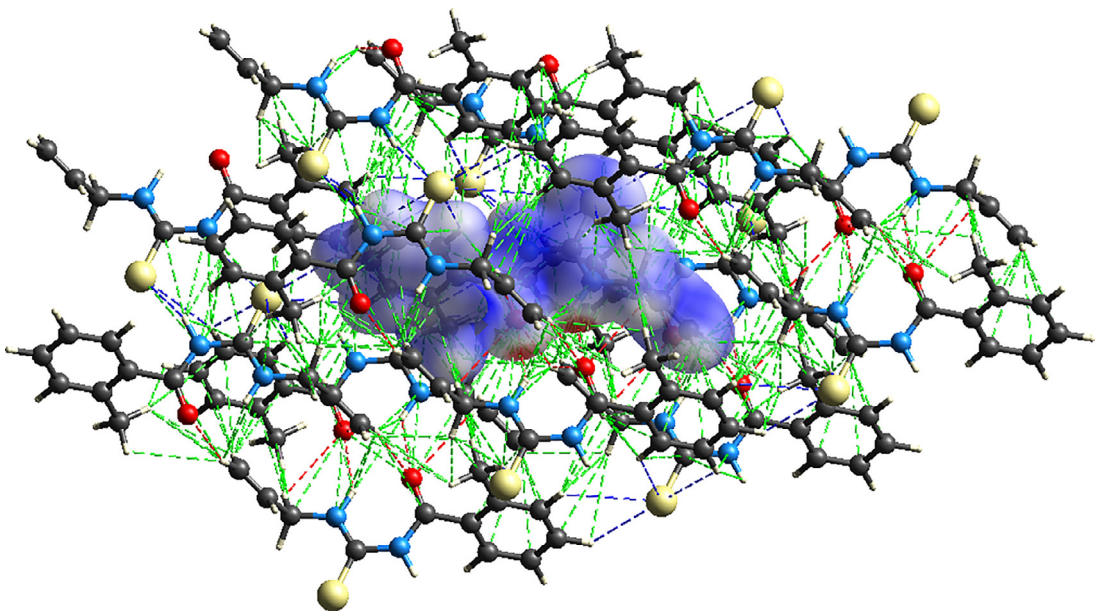

Fig. 14. The non-covalent interactions of HL^2 molecules.

In general, compounds with a smaller HOMO-LUMO energy gap show greater chemical reactivity [50,51]. The HOMO-LUMO band gap values of seventeen different thiourea derivative compounds containing the coumarin thiourea group were calculated and these values were found to be in the 5.05–6.155 eV range [52]. In another report, 1-benzyl-3-(2-furoyl) thiourea was synthesized and HOMO-LUMO band gap was found to be 3.865 eV [53].

Ionization energy and electron affinity can be expressed as: I = -E_{HOMO} and A = -E_{LUMO} [54]. The chemical hardness (η) and chemical potential (μ), are given with the following equations, η= (I-A)/2 and μ= -(I + A)/2, where I and A are the first ionization potential and electron affinity of HL^1 and HL^2 [55]. The values, which were calculated via the given equations, for HL^1 and HL^2 are presented in the Table 6.

In this study, the ionization energy and electron affinity values for HL^1 and HL^2 were found to be I(HL^1)= 0.22653 and 0.30416, A(HL^1)= 0.06641 and 0.00172, I(HL^2)= 0.22477 and 0.30108, and A(HL^2)= 0.06199 and 0.00273 eV, respectively. The chemical hardness and the chemical potential for HL^1 were calculated to be 0.0801 and 0.15122 eV and −0.1465 and −0.15294 eV, respectively. The chemical hardness and chemical potential for HL^2 were calculated to be 0.0814 and 0.14918 eV and - 0.1434 and −0.15191 eV, respectively. The low chemical hardness of both compounds indicates that their chemical activity is high.

The chemical hardness and chemical potential values of 1-(adamantane-1-carbonyl-3-(1-naphthyl)) thiourea ($C_{22}H_{24}N_2OS$) were calculated to be −0.825 eV and −3.075 eV, respectively [50]. Musawwir et al. synthesized seventeen different molecules con-

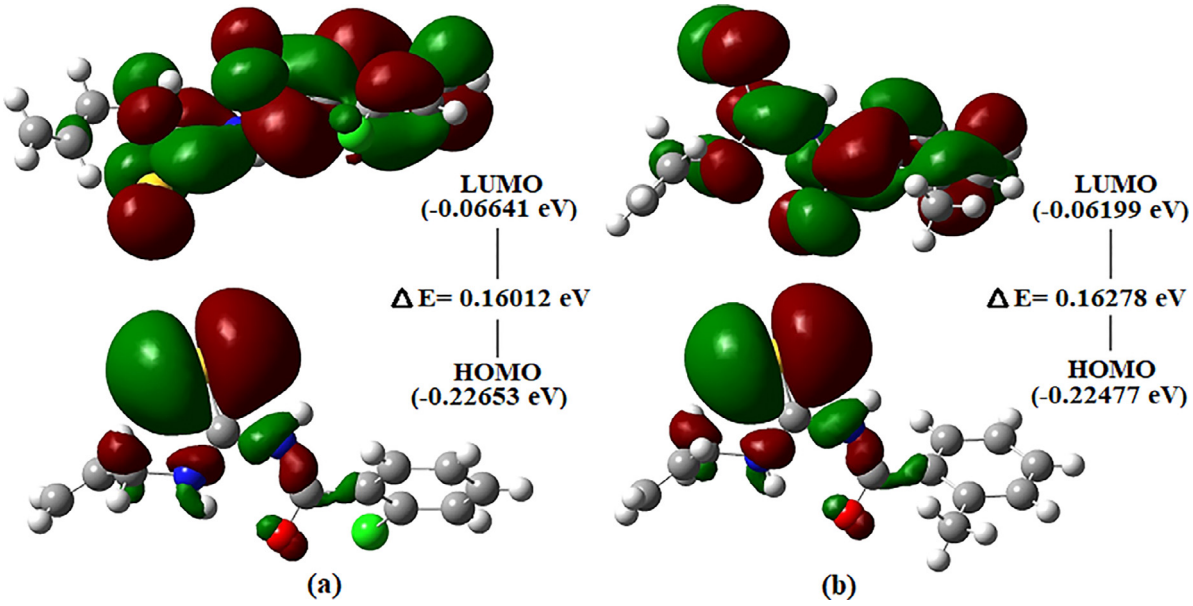

Fig. 15. The HOMO-LUMO orbitals and transition energy values of HL^1(a) and HL^2 (b).

Table 6
The calculated ionization energy (I), electron affinity (A), chemical hardness (η) and chemical potential (μ) values for HL^1 and HL^2.

Calculated	Compound	B3LYP (eV)	ωB97X-D (eV)
Ionization energy (I)	HL^1	0.22653	0.30416
	HL^2	0.22477	0.30108
Electron affinity (A)	HL^1	0.06641	0.00172
	HL^2	0.06199	0.00273
Chemical hardness (η)	HL^1	0.0801	0.15122
	HL^2	0.0814	0.14918
Chemical potential (μ)	HL^1	−0.1465	−0.15294
	HL^2	−0.1434	−0.15191

taining a coumarin thiourea group and performed global reactivity studies. Chemical hardness and chemical potential values of these compounds were calculated in the ranges from 2.525 to 3.2744 eV and from −4.8112 to −4.1498 eV, respectively [52]. Chemical hardness and chemical potantiel values for 1-benzyl-3-(2-furoyl) thiourea are reported to be 1.933 eV and −4.139 eV [53].

3.8. In-silico ADMET prediction

Determining pharmacokinetic properties (i..e, absorption, distribution, metabolism, excretion and toxicity (ADMET)) of chemical compounds is crucial in identifying whether they can be drug molecules or not. These parameters are useful for preventing failure of the targeted compounds in preliminary biological tests and clinical trials and increase their potential to be promising drug candidates [36,56,57]. Rules that show the combination of theoretically and experimentally determined physicochemical properties were used to determine the interactions that the compounds can have after ingestion. The Lipinski Rules (Lipinski's Rule of Five) are one of the ways to evaluate the drug-likeness of compounds or their usability for specific pharmacological and biological activity requirements [58]. The ADME properties of the compounds were evaluated with respect to various parameters (i.e., physicochemical, drug similarity, pharmacokinetic and medicinal chemistry). In accordance with the data obtained and summarized in Table 7, it is concluded that HL^1 and HL^2 obeyed all the Lipinski rules. The HBA, HBD and MR parameters were in good compatibility with each other for both compounds. The estimated water solubility levels of both of the compounds studied were high. The TPSA values have to be less than the critical threshold value of 130. Both HL^1 and HL^2 were found to meet this criteria. The poor ADME properties (e.g., poor absorption of molecule and prolonged first-pass

Table 7
Physicochemical and drug-likeliness properties of synthetic compounds.

		Compound	
	Rule	HL^1	HL^2
MW	<500	254.74	234.32
#H-bond acceptors (HBA)	≤ 9	1	1
#H-bond donors (HBD)	≤ 10	2	2
MR (Molar Refractivity)	<130	68.99	68.94
TPSA	<130	73.22	73.22
Absorption%	>80	83.74	83.74
XLOGP3 (Log Po/w)	≤ 5	2.29	2.37
ESOL Log S		−2.74	−2.67
ESOL Class		Soluble	Soluble
GI absorption		High	High
BBB permeant		Yes	Yes
Pgp substrate		No	No
CYP1A2 inhibitor		Yes	Yes
CYP2C19 inhibitor		Yes	Yes
CYP2C9 inhibitor		Yes	No
CYP2D6 inhibitor		No	No
CYP3A4 inhibitor		No	No
Lipinski #violations		0	0
Ghose #violations		0	0
Veber #violations		0	0
Egan #violations		0	0
Muegge #violations		0	0
Bioavailability Score		0.55	0.55
PAINS #alerts		0	0
Leadlikeness #violations		0	1
Synthetic Accessibility		2.02	1.94

Key: MW: Molecular weight (gr/mol), Abs%: Percentage of absorption, TPSA: Topological polar surface area, RB: number of rotatable bonds, HBA: number of hydrogen bond acceptors, HBD: number of hydrogen bond donors, LV: number of Lipinski rule of 5 violations, Log Po/w (XLOGP3): Lipophilicity, BS: Bioavailability score, SA: Synthetic accessibility [From 1 (very easy) to 10 (very difficult)], WS: Water solubility Log S (Insoluble < −10 <Poorlysssoluble< −6 < Moderately soluble < −4 <Solubale< −2 Very soluble< 0 < Highly soluble) Lipinski RO5: Molecular mass less than 500 Dalton, High lipophilicity (expressed as LogP less than 5), Less than 5 hydrogen bond donors, Less than 10 hydrogen bond acceptors; Molar refractivity should be between 40 -130.

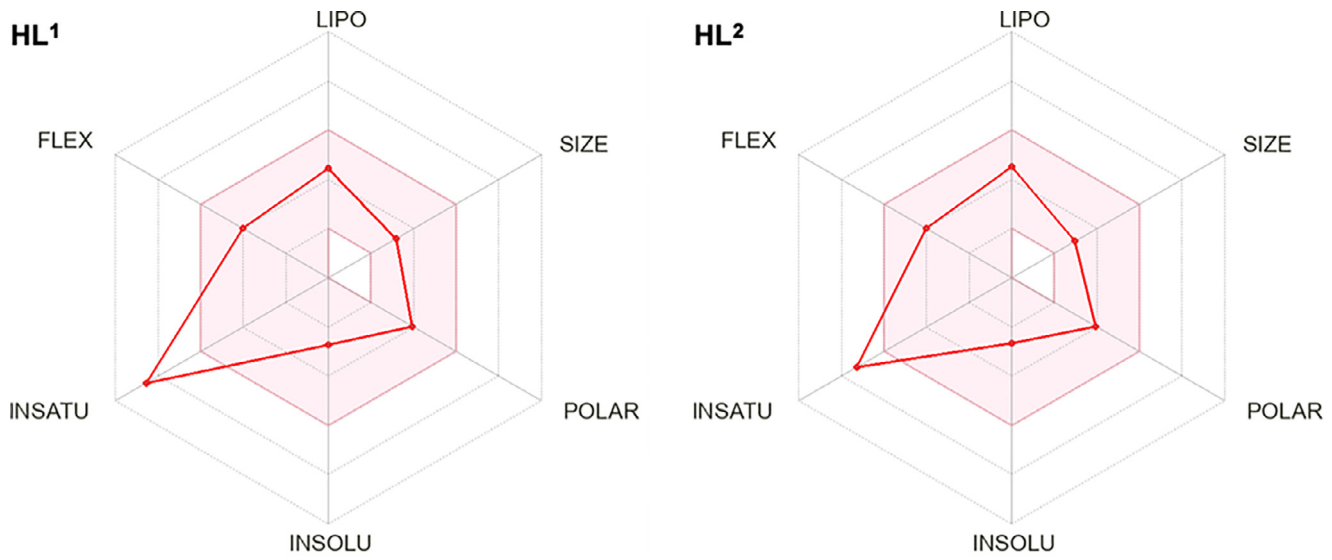

Fig. 16. Bioavailability radar related to the physicochemical properties of compounds.

metabolism) cause many drug candidates to fail in the early stages of drug development.

The absorption value (%) of the compounds was calculated to be 83.74% which is above the lower limit. The permeability of a molecule, which is to be considered as medication, is a crucial parameter in determining its GI absorption and whether it would pass through cell membranes, BBB and other physiological barriers [35]. The CYP refers to a group of enzymes including heme, which is an isoenzyme, catalyzing various oxidation processes. In humans, the primary forms of CYP are CYP2D6, CYP2C9, CYP3A4, CYP1A1, CYP2C19 and CYP2E1, and more than 90% of all drugs on the market undergo at least one of the metabolic processes of the CYP enzymes [30]. It is said that both compounds may be inhibitors of CYP1A2 and CYP2C19. Both compounds were found toobey all of the generally accepted rules (Lipinski, Ghose, Veber, Egan, and Muegge) used for determining whether a compound can be a drug candidate. This indicates that both HL^1 and HL^2 can be potential drug candidates.

The ADME properties of the molecules were visualized via radar plots obtained from the SwissADME website. The radar plots are used to estimate the drug similarity, lipophilicity, size, polarity, solubility, flexibility, and saturation of the compounds. Ideally, these properties of compounds should lie in the pink region indicating their basic properties on the radar graph. The radar plots on the biocompatibility of the compounds are given in Fig. 16. Radar plots show that the synthesized compounds fall entirely into the pink region, except for saturation.

Gastrointestinal absorption and access to brain are the two pharmacokinetic properties critical to predicting the drug development process at various phases. The approach based on Brain or Intestinal Estimated Permeability (Boiled-Egg), which works by measuring the lipophilicity and polarity of small molecules, were presented as an accurate prediction model for this purpose [59]. In the boiled egg model, while the yellow area represents transition to the blood-brain barrier (BBB), the white area indicates absorption in the gastrointestinal (GI) tract. When interpreting the Boiled Egg model, the red dot represents the molecule. If the red dot remains in the outermost gray area, this molecule is not absorbed by the gastrointestinal tract and therefore it cannot cross the blood-brain barrier. The red dot in the white area means that the gastrointestinal absorption is high, but the molecule cannot cross the blood-brain barrier. When the red dot is in the yellow zone, this molecule has high gastrointestinal absorption and can easily cross the blood-brain barrier. When the boiled egg model of both molecules was examined, it was observed that absorption of both compounds in the gastrointestinal tract is highly likely and thus they are expected to cross the blood-brain barrier (Fig. 17).

In addition to the ADME properties of the compounds, their toxicity profiles were investigated in silico. The pkCSMweb tool [31] was used to obtain this information. The lethal dose (LD_{50}), AMES Toxicity, hERG-I and hERG-II inhibitor, human maximum tolerated dose, LOAEL, skin sensitization, *T. pyriformis toxicity*, Hepatotoxicity, and Minnow toxicity of both compounds could be predicted by exploiting this tool. The results of the analysis are given in Table 8.

The AMES test is a bacteria-based method to determine the mutagenic potential of a compound. A positive test result indicates that the substance is mutagenic and might cause cancer. The AMES results were predicted to be negative for both compounds. The maximum recommended tolerated dose (MRTD) measures the threshold for hazardous level of chemicals for humans. For a specific substance, while MRTD values $\leq$0.477 log(mg/kg/day) are considered to be low, values $>$ 0.477 log(mg/kg/day) are considered to be high. These values, which were estimated to be 0.225 and 0.438 log(mg/kg/day) for HL^1 and HL^2, respectively, were below the limit value of 0.477. For hERG I and II Inhibitors, inhibition of potassium channels encoded by hERG (the human Ether-go-go-Related Gene) are the major cause of development of long QT syndrome leading to fatal ventricular arrhythmia. Inhibition of hERG channels lead to withdrawal of many compounds from the pharmaceutical market. These values were estimated as negative for both of the compounds studied. The hazardous potential of a given compound should be tested and analyzed before its use. The lethal dose values (LD_{50}) are widely used as a measure of acute toxicity and is exploited when determining whether a substance is toxic or not. The LD_{50} indicates the amount of a chemical that kills 50% of a set of test specie/animals when given simultaneously. The LD_{50} values were calculated to be 2.427 mol/kg and 2.293 mol/kg for HL^1 and HL^2, respectively. The LOAEL values of these compounds were predicted to be 1.506 and 2.325 log mg/kg_bw/day, respectively.

Drug-induced liver damage is a prominent source of medication attrition and a critical safety concern in drug development. A chemical can be categorized as hepatotoxic if it causes at least one clinical or physiological liver incidence strongly linked to re-

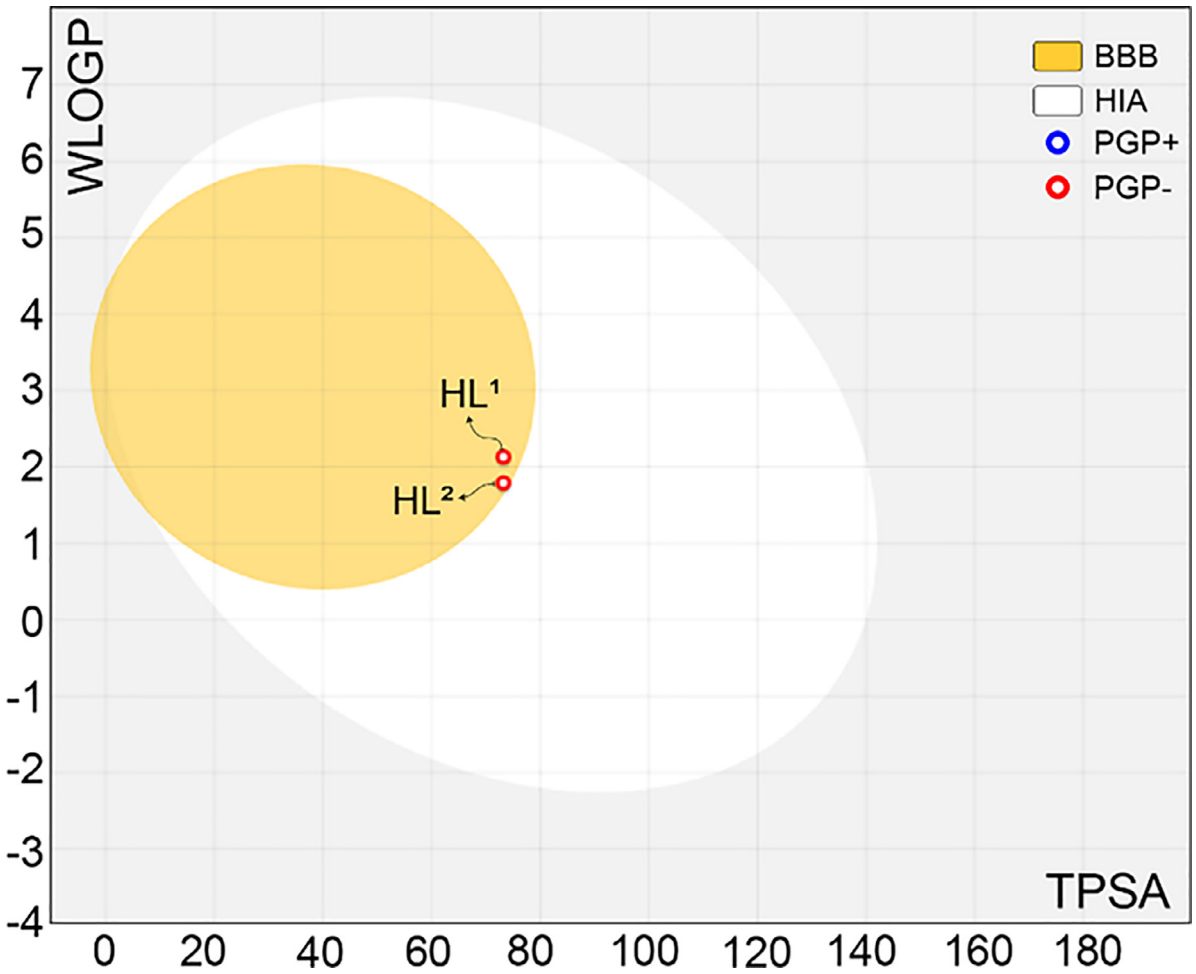

Fig. 17. The Boiled-Egg ADME diagram of the compounds. The yolk region is for those molecules that permeate passively through the blood-brain barrier; the white area represents those molecules that the gastrointestinal tract can passively absorb.

Table 8
Toxicity evaluation of the compounds predicted via thepkCSM server.

	HL^1	HL^2	Unit
AMES toxicity	No	No	Categorical (Yes/No)
Max. tolerated dose (human)	0.225	0.438	Numeric (log mg/kg/day)
hERG I inhibitor	No	No	Categorical (Yes/No)
hERG II inhibitor	No	No	Categorical (Yes/No)
Oral Rat Acute Toxicity (LD50)	2.427	2.293	Numeric (mol/kg)
Oral Rat Chronic Toxicity (LOAEL)	1.506	2.325	Numeric (log mg/kg_bw/day)
Hepatotoxicity	No	No	Categorical (Yes/No)
Skin Sensitisation	Yes	Yes	Categorical (Yes/No)
T.Pyriformis toxicity	0.447	0.271	Numeric (log ug/L)
Minnow toxicity	0.975	1.068	Numeric (log mM)

duced liver function. Both of these compounds were predicted not to show hepatotoxicity. Dermally applied products have the potential to cause skin sensitivity. Both chemicals are expected to cause skin sensitization, given that the pharmacological drug form enters the body dermally. Furthermore, both of the compounds showed T. *pyriformis* toxicity and the values were 0.447 and 0.271 log $\mu g.L^{-1}$ for HL^1 and HL^2, respectively. However, both of these compounds caused very low Minnow toxicity, which has to be 0.5 $mmol.L^{-1}$.

The ProtoxII web server was used to validate the estimated toxicity analysis of the compounds [32]. According to the results obtained, the estimated lethal dose of the HL^1 and HL^2 were calculated to be 2000 mg/kg and 1950 mg/kg, respectively. Moreover, with regard to their overall estimated toxicity, these toxicity level of these compounds was below the moderate level. The Protox toxicity class is measured against a scale ranging from 1 to 6 in 6 different grades. Here, grade 1 is considered to be the most toxic and 6 to be nontoxic. The Protox toxicity values of both compounds, which are given in Table 9, were found to be 4. These values indicate that none of the compounds exhibited immunotoxic effect. None of the compounds were hepatotoxic, immunotoxic, mutagenic nor cytotoxic. The compounds were nontoxic. Only the carcinogenicity value of the compounds was actively monitored, and this value was estimated to be 0.51 which is rather a low value. In general, it can be said that these compounds are not toxic and these values coincide with the outputs obtained via the pkCSM web tool.

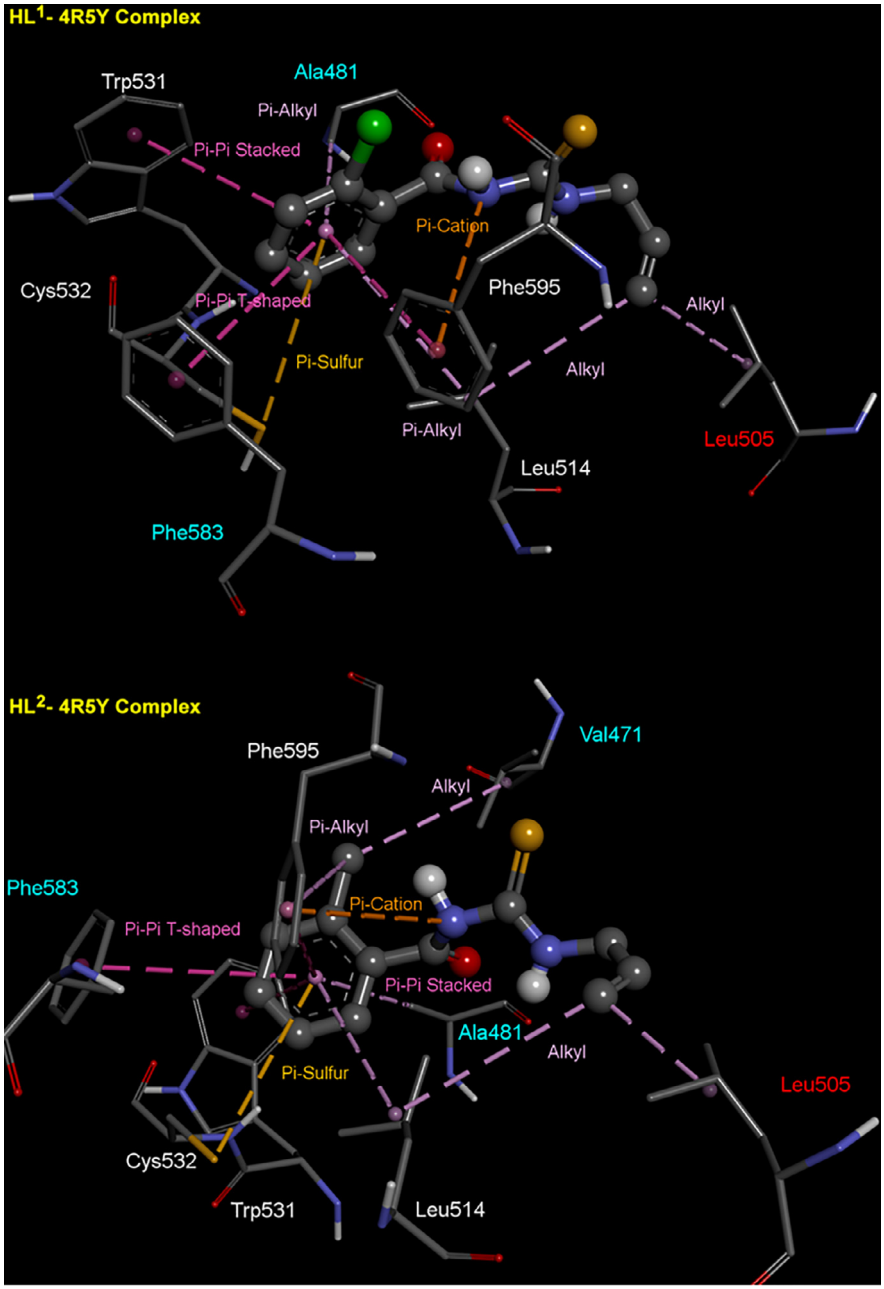

Fig. 18. The 3D representations of the best pose interactions between the BRAF and HL^1 and HL^2. (Bonds indicated by colored dashed lines and types are given in the same colors.).

Table 9
Toxicity model reports of the compounds predicted by the ProTox II server.

	Compound			
	HL^1		HL^2	
Target	Prediction	Probability	Prediction	Probability
Hepatotoxicity	Inactive	0.60	Inactive	0.62
Carcinogenicity	Active	0.51	Active	0.51
Immunotoxicity	Inactive	0.98	Inactive	0.99
Mutagenicity	Inactive	0.55	Inactive	0.67
Cytotoxicity	Inactive	0.73	Inactive	0.71
Predicted LD50	2000 mg/kg		1950 mg/kg	
Predicted Toxicity Class	4		4	

3.9. Molecular docking simulation

Molecular docking analysis –an essential method required for rational drug design- can be eexploited to examine protein-ligand interactions at the atomic level and can predict the most stable structure and the mode of interaction of compounds, allowing for accurate identification and investigation of interaction in drug discovery and development [36,60]. Cancer occurs due to an accumulation of mutations in critical genes that impair normal cell proliferation, differentiation, and death processes. The BRAF protein -a member of the serine–threonine RAF kinase family- is a part of the RAS-RAF-MAPK signaling pathway. This signaling pathway plays an essential role in cell survival, proliferation and differentiation. Activating BRAF mutations uncontrollably activates the MEK-ERK pathway which leads to neoplastic transformation. Among the activating BRAF mutations, it is the most common V600E muta-

Table 10
Summary of the interactions and amino acid residues involved in the inhibition of BRAF.

Score	Interactions	Distance (Å)	Category	Types
−8.1 kcal / mol	:HL1:N1 - A:PHE595	4.85569	Electrostatic	π-Cation
	A:CYS532:SG -:HL1	5.02748	Other	π-Sulfur
	:HL1 - A:TRP531	5.46217	Hydrophobic	π-π Stacked
	:HL1 - A:PHE583	5.59938	Hydrophobic	π-π T-shaped
	:HL1 - A:PHE595	4.82783	Hydrophobic	π-π T-shaped
	:HL1:C11 - A:LEU505	4.47451	Hydrophobic	Alkyl
	:HL1:C11 - A:LEU514	4.77806	Hydrophobic	Alkyl
	:HL1 - A:ALA481	4.30201	Hydrophobic	π-Alkyl
	:HL1 - A:LEU514	5.42971	Hydrophobic	π-Alkyl
−7.9 kcal / mol	:HL2:N1 - A:PHE595	4.84471	Electrostatic	π-Cation
	A:CYS532:SG -:HL2	5.03978	Other	π-Sulfur
	:HL2 - A:TRP531	5.47495	Hydrophobic	π-π Stacked
	:HL2 - A:PHE583	5.60954	Hydrophobic	π-π T-shaped
	:HL2 - A:PHE595	4.82004	Hydrophobic	π-π T-shaped
	:HL2:C9 - A:VAL471	4.77665	Hydrophobic	Alkyl
	:HL2:C12 - A:LEU505	3.31413	Hydrophobic	Alkyl
	:HL2:C12 - A:LEU514	5.09657	Hydrophobic	Alkyl
	:HL2 - A:ALA481	4.04557	Hydrophobic	π-Alkyl
	:HL2 - A:LEU514	5.27288	Hydrophobic	π-Alkyl
	A:PHE595 -:HL2:C9	5.1442	Hydrophobic	π-Alkyl

tion [61]. Somatic-activating BRAF mutations were detected in malignant melanoma, papillary thyroid cancer, colorectal cancer, and lung cancer [62,63]. Therefore, BRAF (V600E) kinase was selected as the target protein, and molecular docking study was performed on the active site of BRAF for the synthesized molecules [64].

After molecular docking studies, the intermolecular interactions between the ligands and the receptor BRAF (4R5Y) were investigated to determine the binding modes of the optimal binding poses. To visualize and compare the binding modes of the compounds, as presented in Fig. 18, the 3D interactions were established. The binding energies of the compounds, the residues with which they interact and the binding types formed are summarized in Table 10. The binding affinity values of the compounds were calculated to be −8.1 and −7.9 kcal/mol for HL^1 and HL^2, respectively. The results obtained were compared with the values of the native ligand (3k3: 5-({(1R,1aS,6bR)−1-[5-(*trifluoromethyl*)−1H-*benzimidazol*-2-*yl*]−1a,6b-dihydro-1H-cyclopropa[*b*][1]benzofuran-5-yl}oxy)−3,4-dihydro-1,8-naphthyridin-2(1H)-one) in the crystal structure of BRAF protein [34]. For this process, the native ligand was re-docking, and the binding affinity was found to be −8.9 kcal/mol. The compounds formed stable complexes via strong interactions at the active site of the target protein. Investigation of the interactions of the compounds in the active pocket of BRAF showed that the types of binding were largely hydrophobic interactions. Both compounds were interacted with the crucial BRAF protein residues -PHE595, ALA481, THR529, and CYS532- to determine whether the protein is active or inactive [61,64]. For most of the BRAF inhibitors, these residues are necessary for tightly binding to the ATP binding site. Since the adenine of the ATP is attached here via Van der Waals forces, the excellent compatibility of these compounds within the hydrophobic pocket (CYS532and ALA481) that binds to ATP, improves the binding affinity of the compounds.

4. Conclusion

The compounds -N-(allylcarbamothioyl)−2-chlorobenzamide (HL^1, $C_{11}H_{11}ClN_2OS$) and N-(allylcarbamothioyl)−2-methylbenzamide (HL^2, $C_{12}H_{14}N_2OS$)- were synthesized and characterized via elemental analysis, DTA-TG, FT-IR and ^1H NMR methods. The molecular structures of the compounds were determined via single-crystal X-ray diffraction. It was observed that both HL^1 and HL^2 crystallize in the triclinic system with the space group *P*-1. The cell similarity value (I_s) for HL^1 and HL^2 was found to be 86.9%. The thermal behavior of the compounds was also examined. The synthesized compounds were thermally stable up to 136 °C and 132 °C, respectively. The DFT analysis for FT-IR was performed with 6–311++*G* (d,p) basis set, B3LYP and ωB97X-D functional. The frequency values obtained as a result of the calculations made with the B3LYP functional in the ν(C = O) bands and the ωB97X-D functional in the ν(C = S) bands were close to the experimental values. The HOMO and LUMO energy levels of HL^1 and HL^2 were calculated using B3LYP and ωB97X-D functional. For HL^1 and HL^2 compounds, values lower than the HOMO-LUMO transition energies reported for similar molecules in the literature were obtained in the calculations made with B3LYP and ωB97X-D functional. The ionization energy, electron affinity, chemical hardness and chemical potential calculations made with these values revealed that the compounds have high chemical activity.

Cytotoxicity activities of the synthesized ligands and their complexes were investigated as well. The cytotoxic effect of the compounds was studied via MTT assay against MCF-7 breast cancer cells. The IC_{50} values for MCF-7 cells were in the range of 2.59–7.09 µmol.L^{-1}. The results indicated that HL^1 at a concentration of 2.59 µmol.L^{-1} was more cytotoxic over a 48 h period. The cytotoxic activity of both compounds was determined to be both dose- and time-dependent. The antitumor activity of HL^1 (when applied for 24 h and 48 h), and of HL^2 (when applied for 24 h) was found to be stronger than that of 5-fluorouracil (5-FU) which is a widely used agent in cancer treatment. The Hirshfeld surfaces analysis of the compounds was performed. The ADMET characteristics of the compounds were widely explored in silico. The results showed that HL^1 and HL^2 obeyed all the Lipinski rules. The HBA, HBD and MR parameters were in good compatibility with each other for both compounds. The estimated water solubility levels of both compounds were high. The TPSA values, which have to be less than the critical threshold value of 130, were found to be low for both HL^1 and HL^2. Moreover, both compounds may be inhibitors of CYP1A2 and CYP2C19. Both compounds were found to obey all of the generally accepted rules (Lipinski, Ghose, Veber, Egan, and Muegge) used for determining whether a compound can be a drug candidate. When the physicochemical, pharmacological, and ADMET properties of HL^1 and HL^2 were compared with respect to drug similarity metrics, it was found that the compounds performed well. Furthermore, molecular docking studies were performed to

assess the interactions between the compounds and BRAF (V600E -protein kinase). The synthesized compounds were shown to have strong binding affinity and inhibitory effect on BRAF (V600E) protein kinase. In the light of the in vitro and in silico data obtained it can be concluded that both of the compounds are potent anticancer agents.

Declaration of Competing Interest

The authors declare that they have no known competing financial interests or personal relationships that could have appeared to influence the work reported in this paper.

CRediT authorship contribution statement

Tuncay Yeşilkaynak: Conceptualization, Methodology, Formal analysis, Investigation, Resources, Writing – original draft, Writing – review & editing, Visualization, Supervision, Project administration, Funding acquisition. **Fatma Nur Özkömeç:** Investigation, Visualization, Data curation. **Mustafa Çeşme:** Investigation, Visualization, Data curation. **Ruken Esra Demirdöğen:** Formal analysis, Resources, Writing – original draft, Writing – review & editing. **Canan Vejselova Sezer:** Investigation, Visualization, Data curation. **Hatice Mehtap Kutlu:** Methodology, Investigation, Resources, Writing – original draft. **Fatih Mehmet Emen:** Investigation, Visualization, Data curation.

Data Availability

Data will be made available on request.

Acknowledgments

The authors thank Kahramanmaraş Sütçü İmam University Scientific Research Projects Unit (*Project codes:* BAP-2019/3–13 M) (Turkey) for funding. Crystallographic data for the structures reported in this paper have been deposited at the Cambridge Crystallographic Data center (CCDC), CCDC 2153424 (HL^1) and CCDC 2153425 (HL^2).

Supplementary materials

Supplementary material associated with this article can be found, in the online version, at doi:10.1016/j.molstruc.2023.135086.

References

[1] Z. Weiqun, Y. Wen, Q. Lihua, Structure and stability of thiourea with water, DFT and MP2 calculations, J. Mol. Struct.: THEOCHEM 730 (2005) 133–141, doi:10.1016/j.theochem.2005.06.012.

[2] K.R. Koch, J.D.S. Miller, O. Seidelmann, Determination of the nucleophilic reactivity constants for a series of N-(n-propyl)-N′-(para-R-benzoyl)thioureas towards trans-[Pt(*pyridine*)2Cl2], Inorganica Chim Acta 331 (2002) 136–142, doi:10.1016/S0020-1693(01)00777-0.

[3] I.B. Douglass, F.B. Dains, The preparation and hydrolysis of mono- and disubstituted benzoylthioureas [1], J. Am. Chem. Soc. 56 (1934) 1408–1409, doi:10.1021/ja01321a061.

[4] C. Sacht, M.S. Datt, Synthesis and characterisation of mixed-ligand platinum(II)–sulfoxide complexes, [PtCl(DMSO)(L)], for potential use as chemotherapeutic agents (HL=N,N-dialkyl-N′-(3-R-benzoyl)thiourea), Polyhedron 19 (2000) 1347–1354, doi:10.1016/S0277-5387(00)00419-8.

[5] X.-P. Rao, Y. Wu, Z.-Q. Song, S.-B. Shang, Z.-D. Wang, Synthesis and antitumor activities of unsymmetrically disubstituted acylthioureas fused with hydrophenanthrene structure, Medic. Chem. Res. 20 (2011) 333–338, doi:10.1007/s00044-010-9303-8.

[6] S. Saeed, N. Rashid, P.G. Jones, M. Ali, R. Hussain, Synthesis, characterization and biological evaluation of some thiourea derivatives bearing benzothiazole moiety as potential antimicrobial and anticancer agents, Eur. J. Med. Chem. 45 (2010) 1323–1331, doi:10.1016/j.ejmech.2009.12.016.

[7] S. Yaseen, M.K. Rauf, S. Zaib, A. Badshah, M.N. Tahir, M.I. Ali, Imtiaz-ud-Din, M. Shahid, J. Iqbal, Synthesis, characterization and urease inhibition, in vitro anticancer and antileishmanial studies of Co(III) complexes with N,N,N′-trisubstituted acylthioureas, Inorganica Chim Acta 443 (2016) 69–77, doi:10.1016/j.ica.2015.12.027.

[8] A. Shakeel, A.A. Altaf, A.M. Qureshi, A. Badshah, Thiourea derivatives in drug design and medicinal chemistry: a short review, J. Drug Des. Medic. Chem. 2 (2016) 10, doi:10.11648/j.jddmc.20160201.12.

[9] H.M. Abosadiya, Synthesis, crystal structure and antioxidant evaluation of N-(4-formylpiperazine-1-carbonothioyl)benzamide, Eur. J. Chem. 11 (2020) 156–159, doi:10.5155/eurjchem.11.2.156-159.1981.

[10] J.R. Burgeson, A.L. Moore, J.K. Boutilier, N.R. Cerruti, D.N. Gharaibeh, C.E. Lovejoy, S.M. Amberg, D.E. Hruby, S.R. Tyavanagimatt, R.D. Allen, D. Dai, SAR analysis of a series of acylthiourea derivatives possessing broad-spectrum antiviral activity, Bioorg. Med. Chem. Lett. 22 (2012) 4263–4272, doi:10.1016/j.bmcl.2012.05.035.

[11] M.K. Rauf, Imtiaz-ud-Din, A. Badshah, M. Gielen, M. Ebihara, D. de Vos, S. Ahmed, Synthesis, structural characterization and in vitro cytotoxicity and anti-bacterial activity of some copper(I) complexes with N,N′-disubstituted thioureas, J. Inorg. Biochem. 103 (2009) 1135–1144, doi:10.1016/j.jinorgbio.2009.05.014.

[12] N.A. Nordin, T.W. Chai, B.L. Tan, C.L. Choi, A.N. Abd Halim, H. Hussain, Z. Ngaini, Novel synthetic monothiourea aspirin derivatives bearing alkylated amines as potential antimicrobial agents, J. Chem. 2017 (2017) 1–7, doi:10.1155/2017/2378186.

[13] D.C. Schroeder, Thioureas, Chem. Rev. 55 (1955) 181–228, doi:10.1021/cr50001a005.

[14] J. Stefanska, D. Szulczyk, A.E. Koziol, B. Miroslaw, E. Kedzierska, S. Fidecka, B. Busonera, G. Sanna, G. Giliberti, P. la Colla, M. Struga, Disubstituted thiourea derivatives and their activity on CNS: synthesis and biological evaluation, Eur. J. Med. Chem. 55 (2012) 205–213, doi:10.1016/j.ejmech.2012.07.020.

[15] G. Binzet, H. Arslan, U. Flörke, N. Külcü, N. Duran, Synthesis, characterization and antimicrobial activities of transition metal complexes of ***N,N*** -dialkyl- ***N′*** -(2-chlorobenzoyl)thiourea derivatives, J. Coord. Chem. 59 (2006) 1395–1406, doi:10.1080/00958970500512633.

[16] V.K. Madan, A.D. Taneja, V.P. Kudesia, Synthesis and spectral studies of some pyrimidyl and thiazolyl substituted thioureas as potential fungicides and nematicides, J. Indian Chem. Soc. 68 (1991) 471–472, doi:10.5281/zenodo.6196766.

[17] G.M. Sheldrick, A short history of SHELX, Acta Crystallogr. A 64 (2008) 112–122, doi:10.1107/S0108767307043930.

[18] C.F. Macrae, I.J. Bruno, J.A. Chisholm, P.R. Edgington, P. McCabe, E. Pidcock, L. Rodriguez-Monge, R. Taylor, J. van de Streek, P.A. Wood, Mercury CSD 2.0 – new features for the visualization and investigation of crystal structures, J. Appl. Crystallogr. 41 (2008) 466–470, doi:10.1107/S0021889807067908.

[19] O.v. Dolomanov, L.J. Bourhis, R.J. Gildea, J.A.K. Howard, H. Puschmann, OLEX2: a complete structure solution, refinement and analysis program, J. Appl. Crystallogr. 42 (2009) 339–341, doi:10.1107/S0021889808042726.

[20] A. Kálmán, L. Párkányi, G. Argay, Classification of the isostructurality of organic molecules in the crystalline state, Acta Crystallogr. B. 49 (1993) 1039–1049, doi:10.1107/S010876819300610X.

[21] P. Bombicz, N.v. May, D. Fegyverneki, A. Saranchimeg, L. Bereczki, Methods for easy recognition of isostructurality – lab jack-like crystal structures of halogenated 2-phenylbenzimidazoles, CrystEngComm 22 (2020) 7193–7203, doi:10.1039/D0CE00410C.

[22] P.R. Spackman, M.J. Turner, J.J. McKinnon, S.K. Wolff, D.J. Grimwood, D. Jayatilaka, M.A. Spackman, CrystalExplorer: a program for Hirshfeld surface analysis, visualization and quantitative analysis of molecular crystals, J. Appl. Crystallogr. 54 (2021) 1006–1011, doi:10.1107/S1600576721002910.

[23] RM, et al., Schlegel H, Scuseria G, Gaussian 09, Revision A.02, Gaussian, Inc., Wallingford CT, 2016.

[24] M.P. McGrath, L. Radom, Extension of Gaussian-1 (G1) theory to bromine-containing molecules, J. Chem. Phys. 94 (1991) 511–516, doi:10.1063/1.460367.

[25] C. Lee, W. Yang, R.G. Parr, Development of the Colle-Salvetti correlation-energy formula into a functional of the electron density, Phys. Rev. B 37 (1988) 785–789, doi:10.1103/PhysRevB.37.785.

[26] J.-D. Chai, M. Head-Gordon, Long-range corrected hybrid density functionals with damped atom–atom dispersion corrections, Phys. Chem. Chem. Phys. 10 (2008) 6615, doi:10.1039/b810189b.

[27] H. Arslan, N. Külcü, U. Flörke, Synthesis and characterization of copper(II), nickel(II) and cobalt(II) complexes with novel thiourea derivatives, Transit. Metal Chem. 28 (2003) 816–819, doi:10.1023/A:1026064232260.

[28] T. Yeşilkaynak, 2-Chloro-N-((5-chloropyridine-2-yl)carbamothioyl)benzamide and its Co(II), Ni(II) and Cu(II) metal complexes: synthesis, characterization, thermal decomposition, electrochemical behavior and antioxidant activity, J. Therm. Anal. Calorim. 124 (2016) 1029–1037, doi:10.1007/s10973-015-5221-9.

[29] J. Han, T.P.N. Talorete, P. Yamada, H. Isoda, Anti-proliferative and apoptotic effects of oleuropein and hydroxytyrosol on human breast cancer MCF-7 cells, Cytotechnology 59 (2009) 45–53, doi:10.1007/s10616-009-9191-2.

[30] A. Daina, O. Michielin, V. Zoete, SwissADME: a free web tool to evaluate pharmacokinetics, drug-likeness and medicinal chemistry friendliness of small molecules, Sci. Rep. 7 (2017) 1–13, doi:10.1038/srep42717.

[31] D.E.V. Pires, T.L. Blundell, D.B. Ascher, pkCSM: predicting small-molecule pharmacokinetic and toxicity properties using graph-based signatures, J. Med. Chem. 58 (2015) 4066–4072, doi:10.1021/acs.jmedchem.5b00104.

[32] P. Banerjee, A.O. Eckert, A.K. Schrey, R. Preissner, ProTox-II: a webserver for the prediction of toxicity of chemicals, Nucleic. Acids. Res. 46 (2018) W257–W263, doi:10.1093/NAR/GKY318.

[33] S. Dallakyan, A.J. Olson, Small-molecule library screening by docking with PyRx, in: J.E. Hempel, C.H. Williams, C.C. Hong (Eds.), Methods in Molecular

Biology, Springer New York, New York, NY, 2015, pp. 243–250, doi:10.1007/978-1-4939-2269-7_19.
[34] M. Çeşme, 2-Aminophenol-based ligands and Cu(II) complexes: synthesis, characterization, X-ray structure, thermal and electrochemical properties, and in vitro biological evaluation, ADMET study and molecular docking simulation, J. Mol. Struct. 1271 (2023) 134073, doi:10.1016/j.molstruc.2022.134073.
[35] İ. Şahin, M. Çeşme, F.B. Özgeriş, Ö. Güngör, F. Tümer, Design and synthesis of 1,4-disubstituted 1,2,3-triazoles: biological evaluation, in silico molecular docking and ADME screening, J. Mol. Struct. 1247 (2022) 131344, doi:10.1016/j.molstruc.2021.131344.
[36] İ. Şahin, M. Çeşme, N. Yüce, F. Tümer, Discovery of new 1,4-disubstituted 1,2,3-triazoles: in silico ADME profiling, molecular docking and biological evaluation studies, J. Biomol. Struct. Dyn. (2022), doi:10.1080/07391102.2022.2025905.
[37] F. Karipcin, M. Atis, B. Sariboga, H. Celik, M. Tas, Structural, spectral, optical and antimicrobial properties of synthesized 1-benzoyl-3-furan-2-ylmethylthiourea, J. Mol. Struct. 1048 (2013) 69–77, doi:10.1016/j.molstruc.2013.05.042.
[38] D. Ugur, H. Arslan, N. Külcü, Synthesis, characterization and thermal behavior of 1,1-dialkyl-3-(4-(3,3- dialkylthioureidocarbonyl)-benzoyl)thiourea and its Cu(II), Ni(II), and Co(II) complexes, Russian J. Coordination Chem./Koordinatsionnaya Khimiya 32 (2006) 669–675, doi:10.1134/S1070328406090089.
[39] M.F. Emen, H. Arslan, N. Külcü, U. Flörke, N. Duran, Synthesis, characterization and antimicrobial activities of some metal complexes with N′-(2-chloro-benzoyl)thiourea ligands: the crystal structure of fac- [CoL3] and cis-[PdL2], Pol. J. Chem. 79 (2005) 1615–1626.
[40] T. Yeşilkaynak, C. Özpınar, F.M. Emen, B. Ateş, K. Kaya, N -((5-chloropyridin-2-yl)carbamothioyl)furan-2-carboxamide and its Co(II), Ni(II) and Cu(II) complexes: synthesis, characterization, DFT computations, thermal decomposition, antioxidant and antitumor activity, J. Mol. Struct. 1129 (2017) 263–270, doi:10.1016/j.molstruc.2016.09.083.
[41] T. Yeşilkaynak, R.E. Demirdöğen, H. Muslu, F.M. Emen, Co(II), Ni(II), and Cu(II) metal complexes based on thiourea ligand: synthesis, characterization, thermal behaviors, anticancer, and antioxidant activities, Inorg. Nano-Metal Chem. (2021) 1–11, doi:10.1080/24701556.2021.1984532.
[42] A. Mohamadou, I. Déchamps-Olivier, J.P. Barbier, Copper, nickel and cobalt complexes with N,N-disubstituted′-benzoyl thioureas, Polyhedron 13 (1994) 1363–1370, doi:10.1016/S0277-5387(00)81702-7.
[43] T. Yeşilkaynak, F.N. Özkömeç, M. Çeşme, R.E. Demirdöğen, E. Kutlu, H.M. Kutlu, F.M. Emen, Synthesis of new thiourea derivatives and metal complexes: thermal behavior, biological evaluation, in silico ADMET profiling and molecular docking studies, J. Mol. Struct. 1269 (2022) 133758, doi:10.1016/j.molstruc.2022.133758.
[44] G. Binzet, F.M. Emen, U. Flörke, T. Yeilkaynak, N. Külcü, H. Arslan, 4-Chloro-N-[N-(6-*methyl*-2-*pyridyl*)*carbamothioyl*]benzamide, Acta Crystallogr. Sect. E Struct. Rep. Online 65 (2008), doi:10.1107/S1600536808041123.
[45] H. Arslan, U. Flörke, N. Külcü, M.F. Emen, Journal of Coordination Chemistry Crystal structure and thermal behaviour of copper(II) and zinc(II) complexes with N-pyrrolidine-N′-(2-chloro-benzoyl)thiourea, (n.d.). https://doi.org/10.1080/00958970500270992.
[46] G. Binzet, H. Arslan, U. Flörke, N. Külcü, N. Duran, Synthesis, characterization and antimicrobial activities of transition metal complexes of N,N-dialkyl-N′-(2-chlorobenzoyl)thiourea derivatives, J. Coord. Chem. 59 (2006) 1395–1406, doi:10.1080/00958970500512633.
[47] W. Liu, J. Zhou, T. Zhang, H. Zhu, H. Qian, H. Zhang, W. Huang, R. Gust, Design and synthesis of thiourea derivatives containing a benzo[5,6]cyclohepta[1,2-*b*]pyridine moiety as potential antitumor and anti-inflammatory agents, Bioorg. Med. Chem. Lett. 22 (2012) 2701–2704, doi:10.1016/J.BMCL.2012.03.002.
[48] A. Saeed, S.A. Ejaz, A. Khalid, P.A. Channar, M. Aziz, T.A. Wani, S. Zargar, S. Hassan, H. Ismail, D. Khalid, M.Z. Hashmi, T. Hökelek, A.T. Aborode, Facile synthesis, crystal structure, biological evaluation, and molecular modeling studies of N-((4-acetyl phenyl) carbamothioyl) pivalamide as the multitarget-directed ligand, Front. Chem. 10 (2022), doi:10.3389/fchem.2022.992701.
[49] B. Arslan, G. Binzet, Synthesis, crystal structure analysis, DFT calculations, antioxidant and antimicrobial activity of N,N-di-2,4-dimethoxybenzyl-N'-2-nitrobenzoylthiourea, J. Mol. Struct. 1267 (2022) 133579, doi:10.1016/j.molstruc.2022.133579.
[50] N. Arshad, A. Saeed, F. Perveen, R. Ujan, S.I. Farooqi, P.Ali Channar, G. Shabir, H.R. El-Seedi, A. Javed, M. Yamin, M. Bolte, T. Hökelek, Synthesis, X-ray, Hirshfeld surface analysis, exploration of DNA binding, urease enzyme inhibition and anticancer activities of novel adamantane-naphthyl thiourea conjugate, Bioorg. Chem. 109 (2021) 104707, doi:10.1016/j.bioorg.2021.104707.
[51] R. Gandhaveeti, R. Konakanchi, P. Jyothi, N.S.P. Bhuvanesh, S. Anandaram, Unusual coordination mode of aroyl/acyl thiourea ligands and their π-arene ruthenium (II) piano-stool complexes: synthesis, molecular geometry, theoretical studies and biological applications, Appl. Organomet. Chem. 33 (2019) e4899, doi:10.1002/aoc.4899.
[52] A. Musawwir, A. Farhat, R.A. Khera, A.R. Ayub, J. Iqbal, Theoretical and computational study on electronic effect caused by electron withdrawing/electron-donating groups upon the coumarin thiourea derivatives, Comput. Theor. Chem. 1201 (2021) 113271, doi:10.1016/j.comptc.2021.113271.
[53] D.M. Gil, M.E. Defonsi Lestard, O. Estévez-Hernández, J. Duque, E. Reguera, Quantum chemical studies on molecular structure, spectroscopic (IR, Raman, UV–Vis), NBO and Homo–Lumo analysis of 1-benzyl-3-(2-furoyl) thiourea, Spectrochim. Acta A Mol. Biomol. Spectrosc. 145 (2015) 553–562, doi:10.1016/j.saa.2015.02.071.
[54] S.H.R. Sebastian, M.A. Al-Alshaikh, A.A. El-Emam, C.Y. Panicker, J. Zitko, M. Dolezal, C. VanAlsenoy, Spectroscopic, quantum chemical studies, Fukui functions, in vitro antiviral activity and molecular docking of 5-chloro-N-(3-nitrophenyl)pyrazine-2-carboxamide, J. Mol. Struct. 1119 (2016) 188–199, doi:10.1016/j.molstruc.2016.04.088.
[55] R.G. Parr, R.G. Pearson, Absolute hardness: companion parameter to absolute electronegativity, J. Am. Chem. Soc. 105 (1983) 7512–7516, doi:10.1021/ja00364a005.
[56] İ. Şahin, F.B. Özgeriş, M. Köse, E. Bakan, F. Tümer, Synthesis, characterization, and antioxidant and anticancer activity of 1,4-disubstituted 1,2,3-triazoles, J. Mol. Struct. 1232 (2021) 130042, doi:10.1016/j.molstruc.2021.130042.
[57] D.K. Isika, F.N. Özkömeç, M. Çeşme, O.A. Sadik, Synthesis, biological and computational studies of flavonoid acetamide derivatives, RSC Adv. 12 (2022) 10037–10050, doi:10.1039/D2RA01375D.
[58] C.A. Lipinski, F. Lombardo, B.W. Dominy, P.J. Feeney, Experimental and computational approaches to estimate solubility and permeability in drug discovery and development settings, Adv. Drug. Deliv. Rev. 46 (2001) 3–26, doi:10.1016/S0169-409X(00)00129-0.
[59] A. Daina, V. Zoete, A boiled-egg to predict gastrointestinal absorption and brain penetration of small molecules, ChemMedChem (2016) 1117–1121, doi:10.1002/cmdc.201600182.
[60] D. Isika, M. Çeşme, F.J. Osonga, O.A. Sadik, Novel quercetin and apigenin-acetamide derivatives: design, synthesis, characterization, biological evaluation and molecular docking studies, RSC Adv. 10 (2020) 25046–25058, doi:10.1039/d0ra04559d.
[61] H.B. El-Nassan, Recent progress in the identification of BRAF inhibitors as anticancer agents, Eur. J. Med. Chem. 72 (2014) 170–205, doi:10.1016/j.ejmech.2013.11.018.
[62] H.S.C. Tang, Y.C. Chen, Insight into molecular dynamics simulation of BRAF(V600E) and potent novel inhibitors for malignant melanoma, Int. J. Nanomed. 10 (2015) 3131–3146, doi:10.2147/IJN.S80150.
[63] J. Kim, B. Choi, D. Im, H. Jung, H. Moon, W. Aman, J.-M. Hah, Computer-aided design and synthesis of 3-carbonyl-5-phenyl-1H-pyrazole as highly selective and potent BRAFV600E and CRAF inhibitor, J. Enzyme Inhib. Med. Chem. 34 (2019) 1314–1320, doi:10.1080/14756366.2019.1599366.
[64] J.J. Liu, H. Zhang, J. Sun, Z.C. Wang, Y.S. Yang, D.D. Li, F. Zhang, H. bin Gong, H.L. Zhu, Synthesis, biological evaluation of novel 4,5-dihydro-2H-pyrazole 2-hydroxyphenyl derivatives as BRAF inhibitors, Bioorg. Med. Chem. 20 (2012) 6089–6096, doi:10.1016/J.BMC.2012.08.020.